



# The 3'UTR of human MAVS mRNA contains multiple regulatory elements for the control of protein expression and subcellular localization

Ling Xu<sup>a,b,c,1</sup>, Li Peng<sup>a,d,1</sup>, Tianle Gu<sup>a,d</sup>, Dandan Yu<sup>a,b,c</sup>, Yong-Gang Yao<sup>a,b,c,d,e,\*</sup>

<sup>a</sup> Key Laboratory of Animal Models and Human Disease Mechanisms of the Chinese Academy of Sciences & Yunnan Province, Kunming Institute of Zoology, Kunming, Yunnan 650223, China

<sup>b</sup> Center for Excellence in Animal Evolution and Genetics, Chinese Academy of Sciences, Kunming, Yunnan 650223, China

<sup>c</sup> Kunming Primate Research Center of the Chinese Academy of Sciences, Kunming Institute of Zoology, Chinese Academy of Sciences, Kunming 650223, China

<sup>d</sup> Kunming College of Life Science, University of Chinese Academy of Sciences, Kunming, Yunnan 650204, China

<sup>e</sup> KIZ – CUHK Joint Laboratory of Bioresources and Molecular Research in Common Diseases, Kunming Institute of Zoology, Chinese Academy of Sciences, Kunming, Yunnan 650223, China

## ARTICLE INFO

### Keywords:

MAVS  
3'UTR  
Antiviral immune  
Regulation mechanism  
Subcellular localization

## ABSTRACT

Post-transcriptional regulation controls the mRNA stability, translation efficiency, and subcellular localization of a protein. The mitochondrial antiviral signaling protein (MAVS) plays a vital role in innate antiviral immunity. The MAVS mRNA has a long 3' untranslated region (UTR, > 9 kb) and an understanding of this region may help to explain the post-transcriptional regulation in a key protein. In this study, we aimed to characterize the role of the MAVS 3'UTR during MAVS expression by truncating the 3'UTR into different fragments so as to identify the regulatory elements. We found that the different fragments (H1–H5) of the MAVS 3'UTR play different roles in regulating the subcellular localization and function of MAVS. Three AU-rich elements (AREs) in the MAVS 3'UTR H1 fragment (region 1–3445 in the 3'UTR) repressed MAVS expression by interacting with HuR to destabilize its mRNA. The MAVS 3'UTR H5 fragment (region 5955–7687 in the 3'UTR) affected the cellular localization of MAVS in mitochondria and influenced the subsequent antiviral function. Four miR-27a binding sites were recognized in the MAVS 3'UTR, and treatment of miR-27a inhibited MAVS expression and promoted the replication of the vesicular stomatitis virus (VSV). The identification of multiple regulatory elements in the MAVS 3'UTR offers new insights into the precise control of MAVS expression in innate immunity.

## 1. Introduction

The innate immune system is the first line of defense against attack by pathogens [1]. A key feature of the innate antiviral immune response is the synthesis and secretion of type I interferons (IFN), such as IFN- $\alpha$  and IFN- $\beta$ , which have antiviral, anti-proliferative and immunomodulatory functions [2]. Recent research has indicated that the mitochondrion acts as a crucial platform for antiviral immunity in vertebrates [3]. Mitochondrial-mediated antiviral immunity is transduced by the activation of the retinoic acid-inducible gene I (RIG-I)-like receptor signal transduction pathway and the participation of the mitochondrial outer membrane adaptor protein MAVS (mitochondrial antiviral signaling protein) [4] [also known as IPS-1 (IFN- $\beta$  promoter stimulator 1) [5], CARDIF (CARD-adaptor-inducing IFN- $\beta$ ) [6], or VISA (virus-induced signaling adaptor) [7]]. MAVS signaling transduction

activates downstream IRF3/7 (interferon regulatory factors 3 and 7) and NF- $\kappa$ B, leading to production of type I IFNs and inflammatory cytokines. Previous studies have shown that MAVS not only plays a pivotal role in the antiviral and inflammatory pathways but is also activated by other regulators and RNA viruses [8]. The expression of MAVS, and its isoforms, is under strict regulation during an innate antiviral immunity response [9–11].

Eukaryotic gene expression involves a series of robust and precise regulation stages including transcription, post-transcription and translation [12–14]. Most mRNA-containing regulatory elements, such as *cis*-acting factors or *trans*-acting factors, are located in the 5' and 3' untranslated regions (UTR). The regulatory elements, such as the AU-rich elements (AREs) are specifically recognized by binding elements including the RNA-binding proteins (RBPs) or RNAs. Their interplay is crucial for the post-transcriptional control of gene expression [12],

\* Corresponding author at: Key Laboratory of Animal Models and Human Disease Mechanisms, Kunming Institute of Zoology, Chinese Academy of Sciences, Kunming, Yunnan 650223, China.

E-mail address: [yaoyg@mail.kiz.ac.cn](mailto:yaoyg@mail.kiz.ac.cn) (Y.-G. Yao).

<sup>1</sup> These authors contributed equally to this work.

<https://doi.org/10.1016/j.bbagrm.2018.10.017>

Received 4 June 2018; Received in revised form 30 October 2018; Accepted 30 October 2018

Available online 01 November 2018

1874-9399/© 2018 Elsevier B.V. All rights reserved.

modulating the mRNA and protein stability [15], or the mRNA transport out of the nucleus and overall translational efficiency [16]. Moreover, UTRs have a fundamental role in the spatial control of gene expression at the post-transcriptional level, which is particularly important during development [17]. The subcellular localization of mRNA is mediated by *cis*-acting elements located in the 3'UTR and in many cases, mRNAs are localized as ribonucleoprotein complexes along with proteins of the translational apparatus, thus ensuring efficient localized translation [18]. MicroRNAs, acting as *trans*-acting elements, bind to the UTRs and regulate the expression of about 60% of human protein-coding genes at the post-transcriptional level by promoting the destabilization/degradation of mRNA and/or inhibition of translation [19–21].

A cross-species analysis has demonstrated that 3'UTRs are substantially longer than the 5'UTRs in most vertebrates, indicating a significant potential for regulation [18]. Moreover, the average length of 3'UTR sequences has increased along with species evolution, suggesting that the 3'UTR might contribute to organism complexity [18]. The transcript of *MAVS* contains several repetitive elements in its 3'UTR, which has a length larger than 9 kb (GenBank accession number [NM\\_020746.3](#)). Given the key role of *MAVS* in antiviral immune signaling, we hypothesized that the 3'UTR of *MAVS* would have a key regulatory role in both physiological and pathological circumstances at the molecular and cellular level. In this study, we systematically characterized the potential regulatory elements in *MAVS* 3'UTR and identified multiple regulatory elements for the control of *MAVS* expression and subcellular localization.

## 2. Materials and methods

### 2.1. Cell lines and viruses

HEK293, Hep G2 and HeLa cells were supplied by the Kunming Cell Bank, Kunming Institute of Zoology (KIZ), Chinese Academy of Sciences (CAS). The cells were grown in Dulbecco's Modified Eagle's medium (DMEM) supplemented with 10% fetal bovine serum (FBS) and  $1 \times$  penicillin/streptomycin (Invitrogen, USA) at 37 °C in 5% CO<sub>2</sub>. Sendai virus (SeV) and vesicular stomatitis virus (VSV) were kind gifts from Dr. Xinwen Chen of the Wuhan Institute of Virology, CAS. Herpes simplex virus-1 (HSV-1) was obtained from Dr. Jumin Zhou's laboratory at the KIZ, CAS. The Newcastle disease virus (NDV) was obtained from the China Institute of Veterinary Drug Control. All the viruses were propagated and amplified following the previously described procedures [22–24].

For the virus infection, HEK293 or HeLa cells were incubated with NDV (MOI = 10), VSV (MOI = 0.001), SeV (25 HAU/mL) or HSV-1 (MOI = 10) for 1 h in DMEM without FBS, respectively, the cells were then rinsed and cultured in fresh medium containing 1% FBS for the indicated times before harvesting.

### 2.2. Plasmid construction

For the epitope-tagged *MAVS* 3'UTR full-length or mutant constructs, the PCR products were cloned into pCS-EGFP (a kind gift from Dr. Bingyu Mao, KIZ) with *BspE* I and *Xba* I, and into psiCHECK-2 vector (Promega, USA) or pBluescript vector (Stratagene, USA) with *Xho* I and *Not* I by using respective primer pairs (Table S1). The miR-27a overexpression vector was cloned into pCMV-MIR (OriGene, USA) with *Sgf* I and *Mlu* I for overexpressing miR-27a precursors (Table S1). The overexpression vector for HuR (HuR-HA) was purchased from the Public Protein/Plasmid Library (#PPL00380-4a, Suzhou, China). The *MAVS* 3'UTR full-length or mutant constructs were generated by multi-sites directed mutagenesis (Stratagene, USA). All constructs were verified by Sanger sequencing.

Three human HuR shRNA lentivirus vectors (shRNA-1, shRNA-2 and shRNA-3) were made by using the pPLK GFP + Puro lentivirus vector

(Public Protein/Plasmid Library) according to the protocol recommended by the manufacturer. The target sequences for human HuR: shRNA-1, 5'-GCAGCATTTGGTGAAGTTGAAT-3'; shRNA-2, 5'-TTGTTAGTGTAACAATCATT-3'; shRNA-3, 5'-CGAGCTCAGAGGTGATCAAAG-3'.

### 2.3. Luciferase reporter assay

HEK293 cells were seeded in 24-well plates at a density of  $0.5 \times 10^5$  cells per well and cultured overnight. The cells were transfected with the *MAVS* 3'UTR full-length or indicated mutant vector (300 ng), the indicated amount of miRNAs by using the Lipofectamine™ 2000 (Invitrogen, USA) for 48 h. The cells were lysed and assessed for luciferase activity by using the Dual-Luciferase Reporter Assay System (Promega, USA) on an infinite M1000 Pro multimode microplate reader (Tecan, USA).

### 2.4. Immunofluorescence analysis

HeLa cells were seeded on glass coverslips and grown overnight to 40% confluence in DMEM medium supplemented with 10% FBS. The cells were co-transfected with pDsRed-mito vector (Clontech, USA, 0.1 µg) and EGFP expression vector (1 µg) with a different *MAVS* 3'UTR fragment (pCS-EGFP-H1, pCS-EGFP-H2, pCS-EGFP-H3, pCS-EGFP-H4 or pCS-EGFP-H5) for 48 h. For the immunofluorescence analysis, the transfected cells were fixed with 4% paraformaldehyde for 10 min and imaged by using an Olympus FluoView™ 1000 confocal microscope (Olympus).

### 2.5. Flow cytometry analysis

HeLa or Hep G2 cells were grown in 12-well plates at a density of  $1 \times 10^5$  cells per well overnight. The cells were transfected with 1 µg of each EGFP expression vector with a *MAVS* 3'UTR fragment (pCS-EGFP-H1, pCS-EGFP-H2, pCS-EGFP-H3, pCS-EGFP-H4, pCS-EGFP-H5, pCS-EGFP-H1-1, pCS-EGFP-H1-2, pCS-EGFP-H1-3, pCS-EGFP-H1-4, pCS-EGFP-H1-5 or pCS-EGFP-H1-6) for 48 h. The cells were then harvested and fixed with 4% paraformaldehyde for 10 min and subjected to flow cytometry analysis on a FACSCalibur (BD Biosciences, USA). The data was analyzed by using FlowJo software (BD Biosciences, USA), and the mean fluorescence intensity and positive percentage rate of green-fluorescing cells were determined.

### 2.6. Western blotting

HEK293 cells were seeded in 6-well plates at  $1 \times 10^6$  cells per well overnight and were transfected with EGFP expression vector with a different *MAVS* 3'UTR fragment (pCS-EGFP-H1, pCS-EGFP-H2, pCS-EGFP-H3, pCS-EGFP-H4 or pCS-EGFP-H5) using X-tremeGENE HP DNA Transfection Reagent (Roche). The cells were lysed on ice in RIPA lysis buffer (Beyotime) and centrifuged at 12,000g at 4 °C for 5 min to collect cell lysates. A total of 30 µg protein were subjected to 12% SDS-PAGE and transferred to polyvinylidene fluoride (PVDF) membranes (Roche) using the standard procedures, as described in our previous studies [23,24]. In brief, the membranes were blocked with 5% non-fat dry milk in Tris-buffered saline (TBS) containing 0.1% Tween 20 (TBST) at room temperature for 2 h, followed by an incubation with the respective primary antibody overnight at 4 °C. We used the following primary antibodies to detect the target proteins: anti-GFP (1: 2000, Enogene) to detect EGFP expression vector with a different *MAVS* 3'UTR fragment (pCS-EGFP-H1, pCS-EGFP-H2, pCS-EGFP-H3, pCS-EGFP-H4 or pCS-EGFP-H5); rabbit anti-VISA (1:1000, Sigma-Aldrich) to detect endogenous *MAVS*; anti-HuR (1:500, Thermo) to detect endogenous HuR, anti-AUF1 (1:1000, Cell Signaling Technology) to detect endogenous AUF1, anti-PARL (1:1000, Abcam) to detect endogenous PARL, anti-GAPDH (1:10,000, Enogene) to detect endogenous GAPDH, anti-ATP5A1 (1:1000, Proteintech) to detect

endogenous ATP5A1, anti-HA (1:5000, Enogene) to detect ectopically expressed HuR tagged by HA (HuR-HA), and anti- $\beta$ -actin (1:10,000, Enogene) to detect endogenous  $\beta$ -actin. The membranes were washed three times with TBST for 5 min each and incubated with anti-mouse or anti-rabbit secondary antibody (1:10,000, KPL, USA) for 1 h at room temperature. After three further washes with TBST, the proteins on the membrane were detected by using enhanced chemiluminescence (ECL) reagents (Millipore, USA).

## 2.7. Mitochondrion isolation

Crude mitochondrion preparations were isolated by using the Mitochondria Crude Isolation Kit (Beyotime, China). About 40  $\mu$ g of crude mitochondria were treated with the indicated amounts of proteinase K for 30 min on ice, followed by a treatment with 1 mM phenylmethylsulfonyl fluoride (Sigma-Aldrich, USA) to stop proteinase K activity. Protein denaturation was performed at 95 °C for 5 min in sodium dodecyl sulfate loading buffer (Beyotime, China) and was subjected to 12% SDS-PAGE using standard procedures for the Western blotting assay.

## 2.8. miRNA mimics and inhibitors

Indicated amounts of miR-27a mimics, miR-326 mimics (dsRNA oligonucleotides) or miR-27a inhibitors, miR-326 inhibitors (single-strand chemically modified oligonucleotides) from Ribobio (Guangzhou, China) were used for overexpressing or inhibiting endogenous miR-27a and miR-326 in HEK293 or HeLa cells, respectively, by using the HiPerFect Transfection Reagent (QIAGEN, USA) according to the manufacturer's instructions. Negative control mimics or inhibitors (Ribobio, Guangzhou) were transfected as matched controls.

## 2.9. Total RNA extraction and reverse-transcription (RT)

Total RNA was extracted from HEK293, HeLa or Hep G2 cells using the RNAsimple Total RNA Kit (TIANGEN, Beijing). The A260/A280 ratio of total RNA was measured on a NanoDrop biophotometer (Thermo Fisher Scientific, USA), and only these RNA samples with a value of 1.8–2.0 were used for subsequent reverse-transcription. We also evaluated the quality and integrity of RNA samples based on the 28S and 18S rRNA bands on a 1% agarose gel. Total RNA (1  $\mu$ g) was used to synthesize cDNA by using the oligo-dT<sub>18</sub> primer and M-MLV reverse transcriptase (Promega, USA). In order to verify the miR-27a expression, 2  $\mu$ g of total RNA was used to synthesize cDNA by using the miR-27a and U6 specific primer. We estimated the half-life of mRNAs using relative mRNA values at four time points (0, 5, 10 and 20 min) following the equation  $\ln M_t = \ln M_0 - \lambda t$ , in which  $M_0$  and  $M_t$  mean the relative mRNA values at 0 min and the indicated  $t$  time point, respectively;  $\lambda$  means the decay rate constant [25].

## 2.10. Reverse transcription quantitative real-time PCR (RT-qPCR)

The RT-qPCR was performed using the SYBR green Premix Ex Taq II (TaKaRa, Dalian) supplemented with gene specific primers (Table S1) on a MyIQ2 Two-Color Real-Time PCR Detection system (Bio-Rad Laboratories, USA), as described in our previous studies [22–24]. The thermal cycling protocol includes 1 cycle at 95 °C for 1 min, 40 cycles of 95 °C for 15 s and 55 °C for 15 s. The resultant PCR products were analyzed by the Bio-Rad software (Bio-Rad, USA). In brief, a volume of 20  $\mu$ L reaction solution containing 0.4  $\mu$ M of each upstream and downstream primer (Table S1), 1  $\mu$ L of cDNA and 10  $\mu$ L of 2  $\times$  SYBR green Premix Ex Taq II, was used for the reaction. The gene expression levels were analyzed using the relative standard curve method. The primers for *MAVS*, *EGFP* and *IFNB1* were shown in Table S1. We treated the total RNA with DNase to remove potential DNA contamination and/or use intron-spanning primers for RT-qPCR. All quantifications were

normalized to the *GAPDH* gene for mRNA expression or U6 for miR-27a normalization.

## 2.11. In vitro transcription and RNA pull-down

The pBluescript vector with the full-length (pBluescript-h) or a *MAVS* 3'UTR fragment (pBluescript-H1, pBluescript-h2 or pBluescript-h3, 3ARE-mutant,  $\Delta$ 957-2145) was digested by the restriction enzyme *Not* I and served as the template for in vitro transcription using the in vitro transcription T7 mMessage Machine Kit (Thermo Fisher Scientific, USA). In brief, the indicated vectors (2  $\mu$ g) were linearized by *Not* I and purified by a QIAquick PCR Purification Kit (Qiagen, Germany). RNA was synthesized by a T7 mMessage Machine Kit (Thermo Fisher Scientific, USA) using the purified linearized-plasmid as the template according to manufacturer's protocol. We treated the RNA with DNase to remove input plasmid. The pull-down assay was performed following the manufacturer's instructions of the Pierce Magnetic RNA-Protein Pull-Down Kit (Thermo Fisher Scientific, USA). Briefly, the target RNAs were biotinylated at the 3' end with a T4 RNA ligase at 16 °C for 4 h. The biotin-labeled RNA (100 pmol) and streptavidin magnetic beads were incubated in a total volume of 100  $\mu$ L for 30 min at room temperature with agitation to form the labeled RNA-beads complex. The cell lysates (200  $\mu$ g) of Hep G2 cells, which were lysed on ice in RIPA lysis buffer (Beyotime), were incubated with the RNA-beads complex at 4 °C for 60 min, followed by washing with elution buffer. The proteins on beads were subjected to Western blot analysis.

## 2.12. Statistical analysis

The differences in relative mRNA and luciferase activity levels between groups with different treatments were calculated using the Student's *t*-test from PRISM software (GraphPad Software, USA). All the data were represented as mean  $\pm$  SEM. In each case, a *P* value < 0.05 was considered to be statistically significant. All statistical analyses were two-tailed, with 95% confidence interval (CI).

## 3. Results

### 3.1. Regulatory elements in the *MAVS* 3'UTR

In order to identify potential regulatory elements in the 3'UTR of *MAVS*, we conducted an *in silico* analysis using UTRdb [26], and found four potential regulatory sites (SXL [Sex-lethal], position 3032-3043; K-box, position 6706-6713 and 8381-8388; BRD-box [Bearded box] at position 1524-1530; the numbering starts from the first nucleotide of the *MAVS* 3'UTR) and several repetitive elements. We then made three different truncated fragments (H1, region 1-3445; h2, region 3380-7041 and h3, region 6029-9976) of 3'UTR and compared them against the full-length construct (Fig. 1A) to characterize the potential function of the elements. Each fragment was cloned into the reporter plasmid psiCHECK-2 (with firefly luciferase as an inner control) at a position downstream of the open reading frame (ORF) of *Renilla* luciferase (Fig. 1A, left). The *Renilla* luciferase activity of psiCHECK-2-H1 was significantly reduced to 10% of that of psiCHECK-2-h with the full-length 3'UTR, implying the existence of regulatory elements in fragment H1. In contrast, psiCHECK-2 vectors containing fragments h2 and h3 had a comparable luciferase activity with the psiCHECK-2-h (Fig. 1A, right).

In order to confirm the potential regulatory elements in 3'UTR, we made truncated fragments (H1–H5) with a shorter length of the *MAVS* 3'UTR and cloned them into pCS-EGFP vector downstream of the EGFP ORF containing two stop codons (Fig. 1B, left). Consistently, HeLa or Hep G2 cells transfected with pCS-EGFP-H1 (region 1-3445) exhibited the lowest percentage of fluorescent cells as compared with that of the pCS-EGFP vector containing another fragment (Fig. 1B and Fig. S1A).

We then focused on fragment H1 (region 1-3445) and further

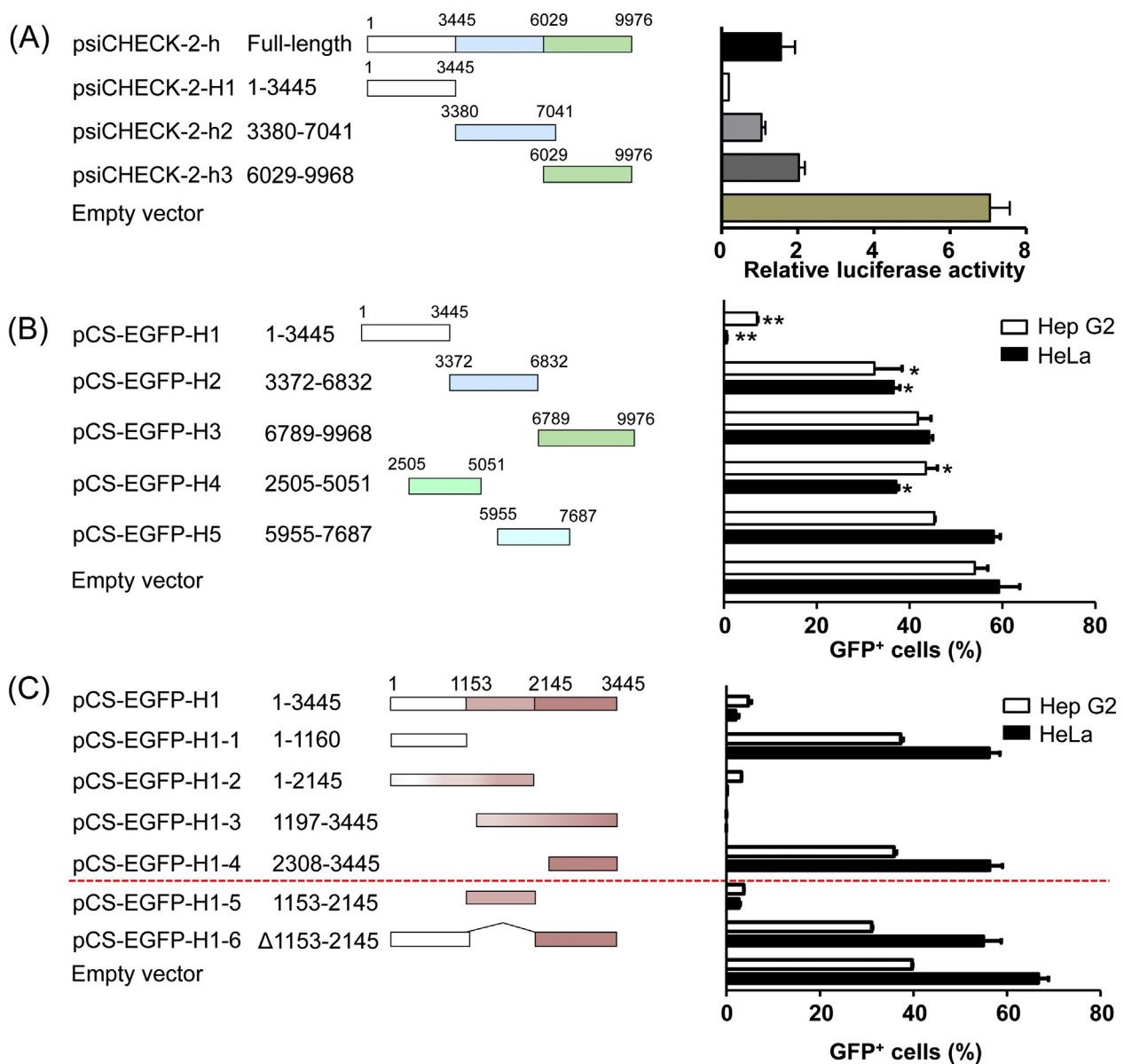


**Fig. 1.** Characterization of the potential regulatory elements in human MAVS 3'UTR. (A) Luciferase reporter analyses of full-length MAVS 3'UTR and its truncated fragments. Schematic profile and location of the full-length (h) or three truncated fragments (H1, h2 and h3) of MAVS 3'UTR were listed on the left. The numbers in the construct name refer to the nucleotide positions in the MAVS 3'UTR, with site 1 being the first nucleotide after the stop codon. The HEK293 cells ( $1 \times 10^5$ ) were transfected with the indicated expression vector (1  $\mu$ g) for 48 h before harvest for quantification of *Renilla* luciferase activity, with a normalization to the firefly luciferase activity as an inner control (Rluc; right). (B) Flow cytometry analyses of cells with transfection of vectors containing MAVS 3'UTR truncated fragments (pCS-EGFP-H1: 1-3445, pCS-EGFP-H2: 3372-6832, pCS-EGFP-H3: 6789-9976, pCS-EGFP-H4: 2505-5051 and pCS-EGFP-H5: 5955-7687). The HeLa or Hep G2 cells ( $1 \times 10^5$ ) were transfected with the indicated expression vector (1  $\mu$ g) for 48 h, then the percentages of GFP-positive cells were quantified by flow cytometry (right). (C) Characterization of the putative inhibitory elements in the MAVS 3'UTR fragment H1. The MAVS 3'UTR fragment H1 was truncated into 5 fragments or introduced with a deletion of 992 bp (left). The procedure was similar to (B). \* $P < 0.05$ , \*\* $P < 0.01$ , Student's *t*-test. Bars represent mean  $\pm$  SEM. All experiments were repeated three times with similar results.

truncated this fragment into 6 smaller fragments (Fig. 1C, left). The putative regulatory elements seemed to be located in region pCS-EGFP-H1-2 (region 1-2145) or pCS-EGFP-H1-3 (region 1197-3445), whereas fragments pCS-EGFP-H1-1 (region 1-1160) and pCS-EGFP-H1-4 (region 2308-3445) had no effect on the EGFP expression. The construct containing a fragment located in region pCS-EGFP-H1-5 (region 1153-2145) caused a decrease of GFP fluorescence, similar to that of pCS-EGFP-H1 (region 1-3445) (Fig. 1C, right and Fig. S1B). Evidently, the MAVS 3'UTR contained elements that negatively influence luciferase reporter activity or GFP expression, and the regulatory element(s) was located in region 1153-2145 of the 3'UTR.

### 3.2. Identification of the AREs in MAVS 3'UTR

The labile mRNAs that encode cytokine and immediate-early gene products often contain AU-rich sequences within the 3'UTR [27]. These AU-rich sequences appear to be key determinants of the short half-life of mRNAs and repress protein translation [28]. The AREs are the most common regulation elements in 3'UTR of mRNA and are responsible for translational repression and mRNA destabilization [29]. We performed a bioinformatics analysis using the AREsite [30] to identify potential *cis*-elements of RNA binding proteins, such as AREs in the MAVS 3'UTR. We identified 11 Class I AREs (AUUUA) in the entire MAVS 3'UTR. Three of them (Site 1: 1080-1084, Site 2: 1201-1205 and Site 3: 2128-

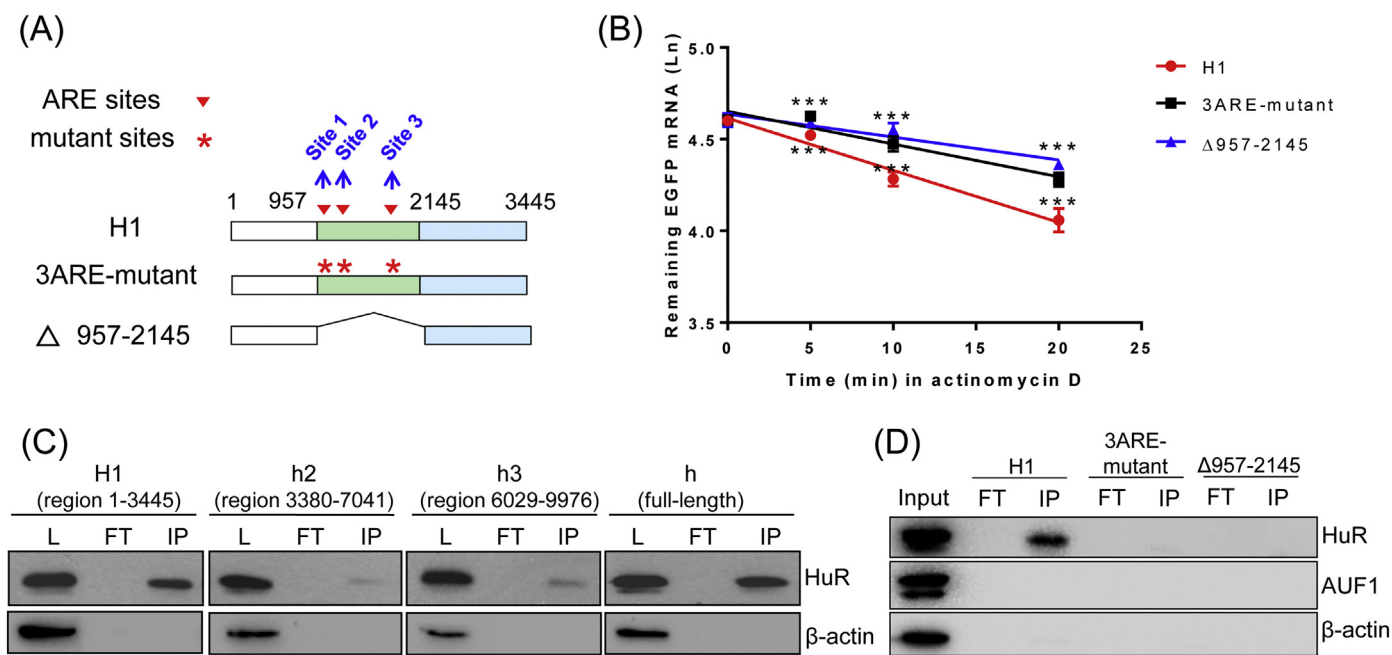


**Fig. 2.** Identification of negative elements in the MAVS 3'UTR and recognition of the RNA-binding protein. (A) Schematic profile of three AU-rich elements (AREs) in human MAVS 3'UTR fragment H1 (region 1-3445) and a mutant with a deletion of region 957-2145 containing three ARE sites. The fragment H1 (vector pCS-EGFP-H1) and its mutants  $\Delta$ 957-2145 (deletion of region 957-2145) and 3ARE-mutant were constructed with the pCS-EGFP vector. (B) Measurement of half-life of EGFP mRNA in transfected HeLa cells. HeLa cells ( $1 \times 10^5$ ) were transfected with the indicated expression vector pCS-EGFP-H1,  $\Delta$ 957-2145 or 3ARE-mutant (1  $\mu$ g) for 24 h, then were treated with or without Actinomycin D (5  $\mu$ g/mL) at the indicated times. Total RNA was extracted from the transfected cells and mRNA level of EGFP was measured by using the quantitative real-time PCR (RT-qPCR), with a normalization to GAPDH. (C) MAVS 3'UTR interacts with the RNA-binding protein HuR. Vectors pBluescript-h, pBluescript-H1, pBluescript-h2 and pBluescript-h3 were used to transcribe full length (h) of MAVS 3'UTR and the fragmented MAVS 3'UTR (H1, h2, and h3) in vitro, respectively. The protein of Hep G2 cells that interacted with the four RNAs were discerned by using the RNA-pull down assay. L - Hep G2 cell lysate, FT - the last wash buffer, IP - the elution buffer containing the RNA-binding proteins. (D) pCS-EGFP-H1 and its mutants interact with the RNA-binding protein HuR, but not AUF1. Vectors pCS-EGFP-H1,  $\Delta$ 957-2145 and 3ARE-mutant were used to transcribe different fragments of MAVS 3'UTR in vitro, respectively. The subsequent procedure was similar as (C). \* $P < 0.05$ , \*\* $P < 0.01$  and \*\*\* $P < 0.001$ , Student's *t*-test. Bars represent mean  $\pm$  SEM. All experiments were repeated three times with similar results.

2132; the numbering starts from the first nucleotide of the MAVS 3'UTR, Fig. S2) were located in region 957-2145 (Fig. 2A). To test whether these three AREs in fragment H1 (region 1-3445) would affect mRNA stability, we deleted a 1188 bp region containing these AREs to make a deletion mutant (vector  $\Delta$ 957-2145) and mutated all three AREs from AUUA to AUCUA in the vector pCS-EGFP-H1 to AUCUA (vector 3ARE-mutant). Intriguingly, removal or mutation of these AREs in fragment H1 significantly increased the half-life of mRNA (Fig. 2B).

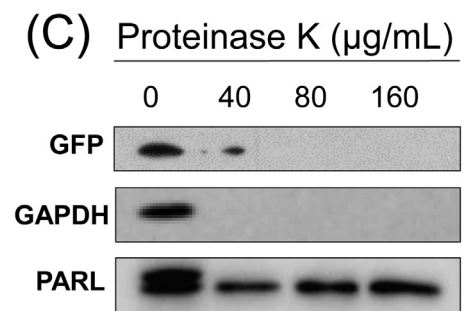
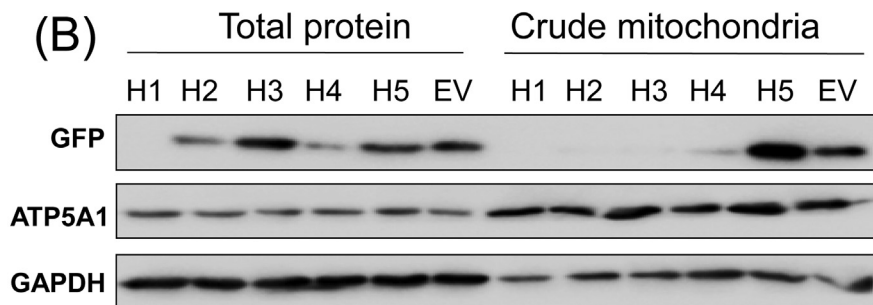
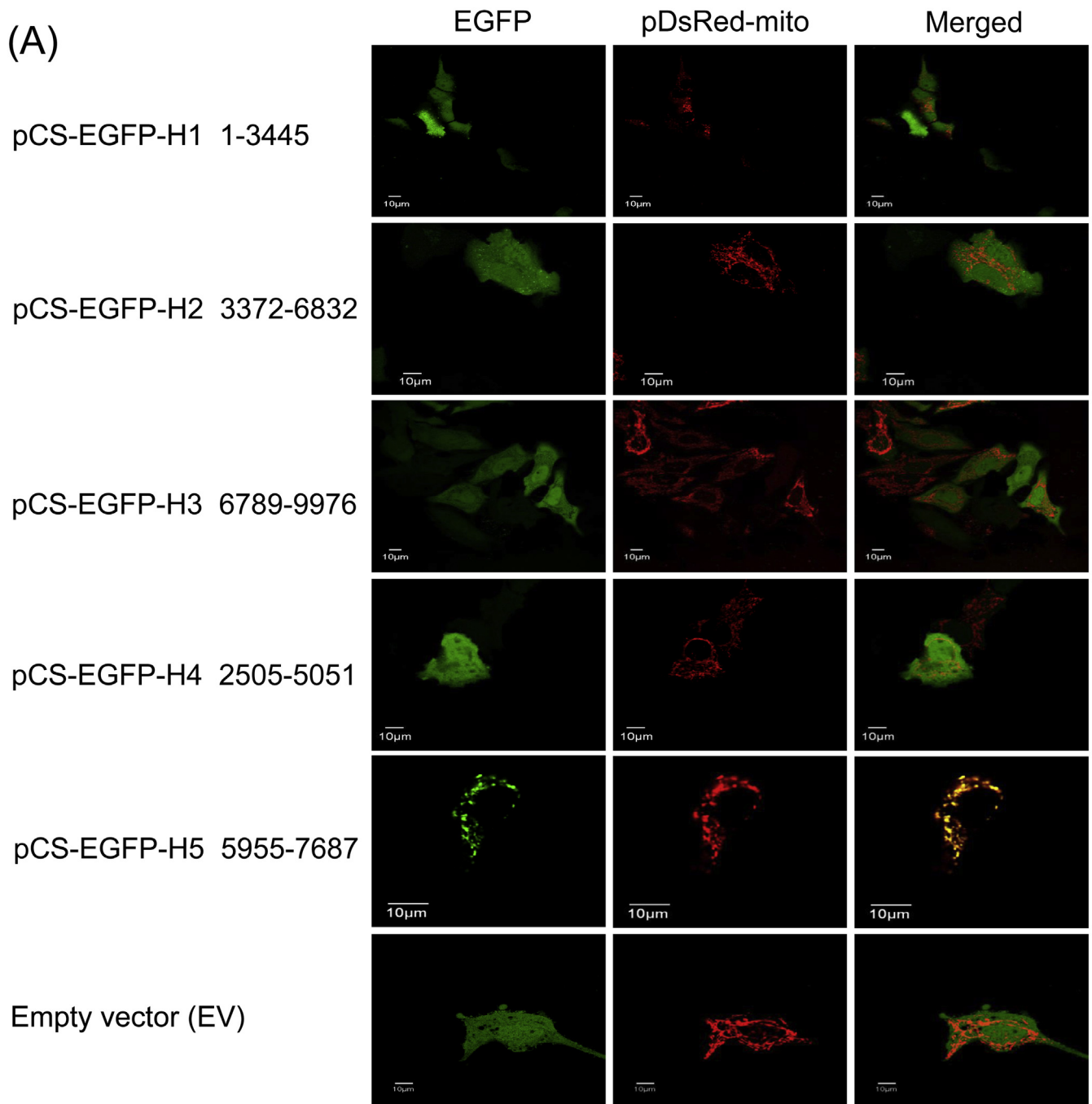
The AREs are recognized by several sequence-specific RBPs, such as HuR, AUF1 and HSP70-1, for binding to many ARE-mRNAs and for assembling other factors into the mRNA degradation machinery [29,31–33]. We performed in vitro transcription and RNA pull-down assays to show the potential involvement of RBPs. HuR could bind to fragment H1 (region 1-3445) and the full-length MAVS 3'UTR, but could barely bind to fragments h2 (region 3380-7041) and h3 (region 6029-9976) (Fig. 2C). Moreover, HuR protein could not interact with  $\Delta$ 957-2145 or 3ARE-mutant relative to the control H1 (region 1-3445) (Fig. 2D), indicating that the AREs are essential for the binding of HuR. However, we found that the RNA-binding protein AUF1, which acts as a cofactor of HuR to promote p16<sup>INK4a</sup> mRNA degradation in a recent report [34], was not involved in the interaction of fragment H1 and HuR (Fig. 2D), suggesting different regulatory roles in this process.

To examine whether the repressive effect of HuR on MAVS expression was affected by viral infection at the cellular level, we assessed the mRNA stability of MAVS in HeLa cells when HuR was overexpressed or was knocked down, together with or without virus infection. Among the three shRNAs for HuR knockdown, shRNA-1 had the highest knockdown efficiency and was used in the subsequent assays (Fig. S3A). Overexpression of HuR (Fig. S3A) remarkably decreased the half-life of MAVS mRNA, regardless of SeV or HSV-1 infection. Consistently,

knockdown of HuR increased the stability of MAVS mRNA (Fig. S3B). Taken together, these results demonstrated that *cis*-elements AREs in the MAVS 3'UTR directly affected mRNA stability, and this effect was dependent on AREs-HuR.

### 3.3. MAVS 3'UTR sorted mRNA to the vicinity of mitochondria

A previous study reported that 3'UTR of mRNAs encoding for mitochondrial proteins have a role in subcellular localization [35]. As MAVS targets to the mitochondrial outer-membrane to initiate signal transduction [4], we tested whether different 3'UTR fragments have different effects on subcellular localization of MAVS. We transfected HeLa cells with the EGFP vector containing each of the five MAVS 3'UTR fragments (H1-H5) and pDsRed-mito vector. In HeLa cells transfected with pCS-EGFP-H5 (region 5955-7687), we observed a colocalization of EGFP with mitochondria, whereas HeLa cells with a transfection of pCS-EGFP-H2 (region 3372-6832) showed a puncta structure diffusely in the cytoplasm (Fig. 3A). We obtained a similar pattern in Hep G2 cells (Fig. S4). The protein expressed from the construct pCS-EGFP-H5 was found in crude mitochondrial fraction isolated from the transfected Hep G2 cells, whereas protein expressed from the other expression vectors was not found in this fraction (Fig. 3B). We treated the crude mitochondria by proteinase K. The expressed GFP via pCS-EGFP-H5 were digested by proteinase K in a dose-dependent manner as we increased the concentrations of proteinase K, in contrast to the mitochondrial integral membrane protein PARL. It is evident that fragment H5 has an effect on cellular transportation of expressed protein to the mitochondria, albeit the transported protein was not completely transported into mitochondria (Fig. 3C). The exact reason for the subcellular localization led by H5 awaits further characterization.



(caption on next page)

**Fig. 3.** MAVS 3'UTR facilitates the transport of mRNA to the vicinity of mitochondria. (A) Localization of EGFP in HeLa cells transfected with pCS-EGFP expression vectors with different fragments of MAVS 3'UTR. Cells ( $1 \times 10^5$ ) were cultured on glass slides in a 12-well plate and were co-transfected with pDsRed-mito vector (0.1  $\mu$ g) and the indicated pCS-EGFP expression vector (1  $\mu$ g) containing the indicated MAVS 3'UTR truncated fragment (pCS-EGFP-H1 1-3445, pCS-EGFP-H2 3372-6832, pCS-EGFP-H3 6789-9976, pCS-EGFP-H4 2505-5051 and pCS-EGFP-H5 5955-7687) or empty vector (EV) for 48 h. Living cells were imaged using the Olympus FluoView 1000 confocal microscope at 488 nm and 563 nm, respectively. (B) Validation of the localized EGFP to mitochondria via the MAVS 3'UTR fragments. The Hep G2 cells ( $1 \times 10^6$ ) were transfected with the indicated pCS-EGFP expression vectors containing MAVS 3'UTR truncated fragments (H1: pCS-EGFP-H1, H2: pCS-EGFP-H2, H3: pCS-EGFP-H3, H4: pCS-EGFP-H4 and H5: pCS-EGFP-H5) or empty vector (EV). Crude mitochondria were isolated from the transfected cells at 48 h. Immunoblots for EGFP, ATP5A1 and GAPDH were performed by using anti-EGFP, anti-ATP5A1 and anti-GAPDH antibodies, respectively. (C) The MAVS 3'UTR fragment H5 directed the expressed protein into mitochondria. The Hep G2 cells ( $1 \times 10^7$ ) were transfected with pCS-EGFP-H5 for 48 h and harvested for isolation of crude mitochondria. Around 20  $\mu$ g of crude mitochondria fraction were treated with 0  $\mu$ g/mL, 40  $\mu$ g/mL, 80  $\mu$ g/mL and 160  $\mu$ g/mL proteinase K for 30 min on ice, respectively, then 1 mM phenylmethylsulfonyl fluoride were added to stop proteinase K reaction. Western blot was performed similar to (B). Mitochondrial protein PARL was used as the positive control.

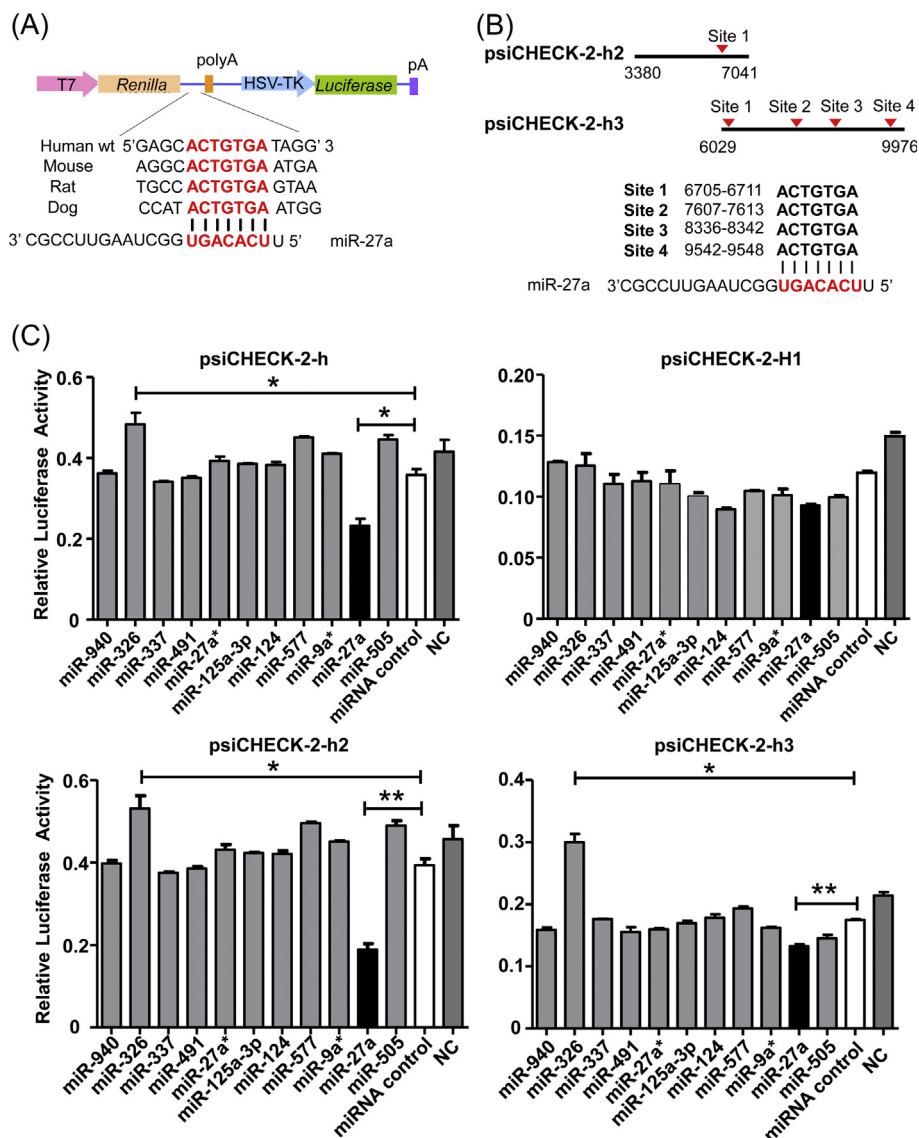


**Fig. 4.** Prediction of miR-27a binding sites in the 3'UTR of MAVS and characterization of its interaction with MAVS 3'UTR. (A) A schematic plot of the luciferase constructs and the conserved miR-27a binding sites in the MAVS 3'UTR of human, mouse, rat and dog. (B) The miR-27a binding sites in fragments h2 and h3 of MAVS 3'UTR. The red labels indicated the miR-27a binding sites in MAVS 3'UTR fragments h2 and h3 that were inserted into psiCHECK-2 vector. (C) The miR-27a repressed the luciferase activity of the psiCHECK-2 vectors containing different MAVS 3'UTR fragments. HEK293 cells ( $1 \times 10^4$ ) were transfected with the indicated reporter vector (psiCHECK-2-h, psiCHECK-2-H1, psiCHECK-2-h2 or psiCHECK-2-h3), along with the indicated miRNA mimics (50 nM), miRNA control (50 nM) or without miRNA (NC), respectively. Cells were lysed and detected for luciferase activity at 48 h after transfection. \*P < 0.05, \*\*P < 0.01, Student's *t*-test. Bars represent mean  $\pm$  SEM. The experiments were repeated three times with similar results.

3.4. Predicted miRNAs interacted with 3'UTR of MAVS mRNA

microRNAs (miRNAs) are an abundant class of small (~22 nt) regulatory RNAs found in plants and animals [36] and play important roles in development by modulating the post-transcriptional regulation of their target genes [19,37,38]. We performed a bioinformatics analysis to identify potential miRNAs that may interact with MAVS. There are several candidate miRNAs predicted by the three different algorithms and databases that were used to predict putative miRNAs targeting the 3'UTR region of MAVS: PicTar (<http://pictar.mdc-berlin.de/>) [39],

TargetScan (<http://www.targetscan.org/>) [40] and miRnada (<http://www.microna.org/microna/home.do>) [41]. The predicted miRNAs were ranked according to the number of putative target sites and the sum of the alignment scores determined by both seed match type and seed match context [19]. We selected 11 miRNAs from the hundreds of these predicted miRNAs for further validation. The full-length 3'UTR or fragments of MAVS were cloned to a luciferase reporter gene in a dual luciferase expression vector (psiCHECK-2) (Fig. 1A) and the vectors were transfected into HEK293 cells. The 3'UTR of MAVS contained four putative miR-27a target sites and the targeted position was highly

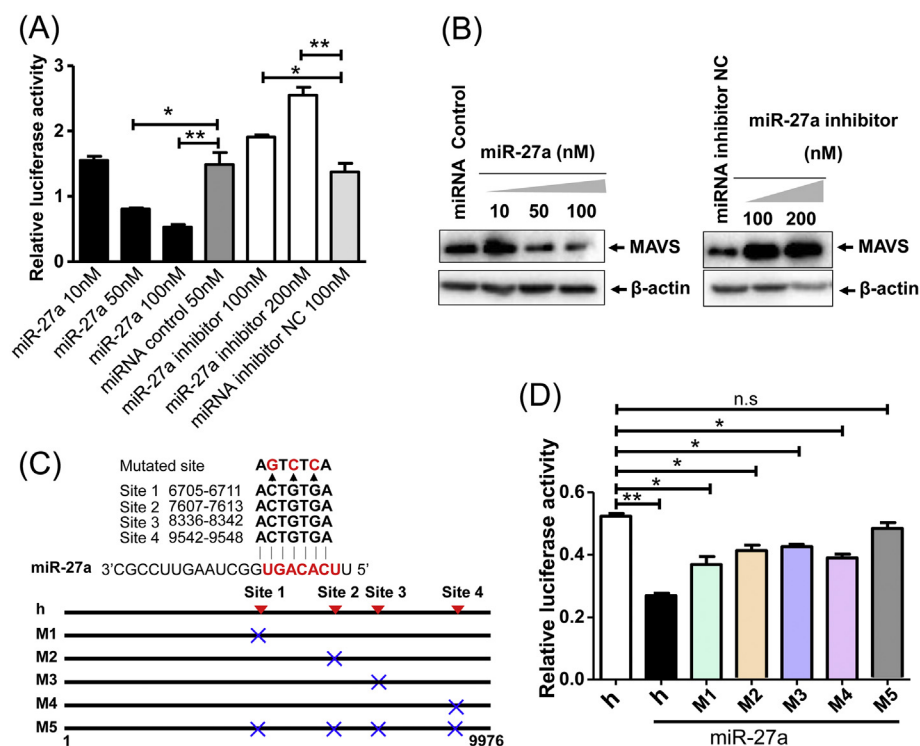


**Fig. 5.** miR-27a directly targets to the MAVS 3'UTR. (A) The inhibitory effect of miR-27a on the MAVS 3'UTR presents a dose-dependent manner. HEK293 cells ( $1 \times 10^4$ ) were transfected with the reporter vector psiCHECK-2-h and different concentrations of miR-27a mimics or miR-27a inhibitors. Cells were lysed and detected for luciferase activity at 48 h after transfection. miRNA control and miRNA inhibitor control (miRNA inhibitor NC) were used as negative controls. (B) Effect of miR-27a on endogenous MAVS protein expression. HeLa cells ( $1 \times 10^5$ ) were transfected with the miR-27a inhibitor (100 nM, 200 nM), miRNA inhibitor NC (100 nM), miRNA control (100 nM) or different concentrations of miR-27a mimics (10 nM, 50 nM and 100 nM). Cells were harvested at 48 h after transfection and the endogenous MAVS was detected by Western blot. Immunoblot for  $\beta$ -actin was used as loading control. (C) Schematic profile of mutants for miR-27a seeding region. Four mutant vectors (M1, M2, M3 and M4) were generated by mutating one of the four seeding regions of miR-27a binding sites in the psiCHECK-2-h vector (h). Mutant expression vector M5 was generated by mutating all seeding region of miR-27a binding sites. The red labels in the schematic structure indicated the miR-27a binding sites in the MAVS 3'UTR; the blue labels indicated the mutated sites. (D) Effects of miR-27a on the luciferase activity of the five mutants of the psiCHECK-2-h vector (h) or the indicated psiCHECK-2-h mutant vector (M1-M5), together with or without miR-27a mimics (50 nM), respectively. Cells were harvested for luciferase activity at 48 h after transfection. n.s. - not significant, \* $P < 0.05$ , \*\* $P < 0.01$ , Student's *t*-test. Bars represent mean  $\pm$  SEM. The experiments were repeated three times with similar results.

conserved among several species (Fig. 4A). Fragment H1 of MAVS 3'UTR contained no miR-27a target sequence, but fragments h2 and h3 contained 1 and 4 miR-27a target sequences, respectively (Fig. 4B). When the miR-27a was added exogenously as miRNA mimics, it significantly reduced the expression of luciferase relative to a negative miRNA (miRNA control) (Fig. 4C). miR-27a mimics markedly decreased the luciferase levels when co-transfected with h2 and h3, but not H1 which had no predicted miR-27a target sequence (Fig. 4C). These results suggested that miR-27a was one of miRNAs binding to MAVS 3'UTR. Note that miR-326 had a significant stimulation effect, with a contrast pattern to that of miR-27a (Fig. 4C and Fig. S5). A focused study will be needed to further characterize the indirect role of miR-326 during the regulation of MAVS expression.

To confirm whether MAVS 3'UTR is a direct target of miR-27a, we co-transfected MAVS 3'UTR vector psiCHECK-2-h with miR-27a mimics or inhibitors. We observed a statistically significant, dose-dependent suppression of luciferase activity by miR-27a, whereas miR-27a inhibitors increased luciferase levels compared with the controls (Fig. 5A). Consistent with the inhibition effect of miR-27a on MAVS expression, transfection of miR-27a mimics decreased MAVS protein level, whereas miR-27a inhibitors increased MAVS expression (Fig. 5B). Mutations that disrupted the miR-27a seed sequence (Fig. 5C) changed their ability to inhibit luciferase activity, especially when all four miR-27a target sites were mutated (Fig. 5D). These results demonstrated that endogenous MAVS mRNA was a direct target of miR-27a via its 3'UTR. Moreover, transfection of miR-326 mimics or miR-326 inhibitor in HEK293 cells led to a dose-dependent enhancing effect on MAVS protein expression (Fig. S5), which was in contrast to the pattern for miR-27a.

### 3.5. Up-regulation of miR-27a inhibited virus-triggered MAVS-dependent *IFNB1* expression and promoted VSV replication

In order to show how the regulatory elements in MAVS 3'UTR enact

a biological function via the modulation of MAVS expression, we took the miR-27a as an example. The mature miR-27a was upregulated following NDV, SeV, VSV or HSV-1 infections (Fig. 6A). After the viral infection, the levels of miR-27a were increased by at least 30% in HeLa cells. We further assessed the MAVS expression in cells with successful overexpression of pCMV-miR-27a vector (Fig. 6B). Overexpression of miR-27a inhibited SeV-, NDV- or HSV-1-induced MAVS mRNA level and protein expression (Fig. 6C), as compared with the pCMV-MIR vector (Empty vector). We noticed that MAVS mRNA was significantly decreased at different time points and different levels in the presence of miR-27a, suggesting that other regulators, such as RNA binding protein (HuR) or other miRNAs were involved in controlling MAVS expression in these conditions.

As MAVS was a critical adaptor to induce downstream signaling for type I IFN response [42], we would expect that miR-27a overexpression had an inhibition effect on *IFNB1* mRNA expression via the mediation of MAVS. We found that overexpression of miR-27a remarkably inhibited SeV-, NDV- or HSV-1-induced mRNA expression level of *IFNB1* (Fig. 6D). Furthermore, overexpression of miR-27a promoted VSV-GFP replication, whereas inhibition of miR-27a suppressed VSV replication (Fig. 6E–F). Evidently, miR-27a negatively regulated the MAVS-dependent IFN production and affected VSV replication, via the modulation of MAVS expression through its 3'UTR.

## 4. Discussion

The regulation of gene expression has been traditionally considered to occur at the transcriptional level, with major roles for transcription factor recruitment/activation and DNA structure at the promoter region [43,44]. Regulation at the post-transcriptional level has been recognized in recent decades, and UTRs in the majority of genes act as important regulatory elements [29]. Considering the complex of different RNA-interacting factors, UTRs can regulate mRNA stability, determine the subcellular localization and control translation efficiency.

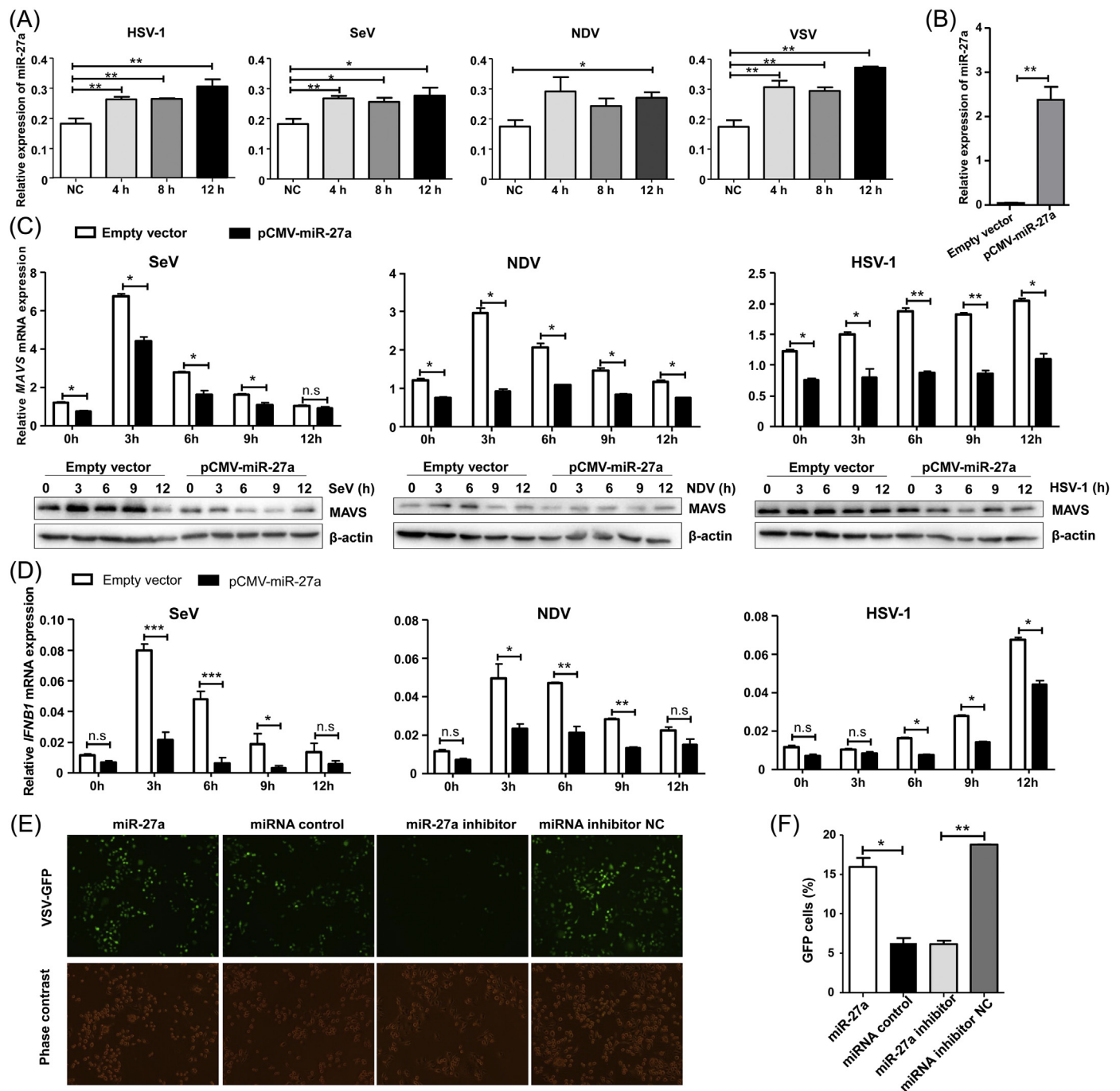


**Fig. 6.** miR-27a was up-regulated in response to virus infections for inhibiting the MAVS-dependent IFN production. (A) Virus infection induces a significant upregulation of the miR-27a level. HeLa cells ( $1 \times 10^4$ ) were infected with HSV-1 (MOI = 10), NDV (MOI = 10), SeV (25 HAU/mL), VSV (MOI = 0.001), or without infection (NC), respectively, and were harvested at the indicated times after infection. Data shown were relative miR-27a levels that were normalized by the U6 levels. (B) Successful overexpression of miR-27a in HeLa cells. Cells ( $1 \times 10^5$ ) were transfected with the pCMV-miR-27a or pCMV-MIR vector (empty vector) (1  $\mu$ g each) for 48 h before the harvest. The level of miR-27a was measured by using the RT-qPCR. (C) Overexpression of miR-27a inhibits the MAVS mRNA and protein levels in response to virus infection. HeLa cells were transfected with the pCMV-miR-27a or pCMV-MIR vector (empty vector) as described in (B) for 36 h, followed by NDV (MOI = 10), HSV-1 (MOI = 10) or SeV (25 HAU/mL) infection for the indicated times. The mRNA expression level of MAVS (upper) was measured by using the RT-qPCR, and the protein levels (below) were quantified by Western blot using antibody for MAVS. The  $\beta$ -actin was used as the loading control. (D) Overexpression of miR-27a inhibits the *IFNB1* mRNA expression in response to virus infection. The procedures for transfection and viral infections were same to (C). (E–F) The miR-27a promotes the replication of VSV. HeLa cells ( $1 \times 10^5$ ) were transfected with miR-27a mimics (50 nM), miRNA control (50 nM), miR-27a inhibitor (100 nM) and miRNA inhibitor control (miRNA inhibitor NC, 100 nM) for 24 h, then were infected with VSV-GFP (MOI = 0.001) for 12 h. The EGFP expression was detected by fluorescence microscope imaging (E) and flow cytometry (F). n.s. - not significant, \* $P < 0.05$ , \*\* $P < 0.01$ , \*\*\* $P < 0.001$ , Student's *t*-test. Bars represent mean  $\pm$  SEM. The experiments were repeated three times with similar results.

Therefore, UTRs could influence the total amount of synthesized protein [45]. This is a reason why in many cases the 3'UTR substantially exceeds the length of the ORF [18] in a mature mRNA. In this study, we characterized the long 3'UTR of MAVS to show the precise regulation of this important protein that plays a key role in antiviral immunity, as another example for post-transcriptional regulation of a gene.

In a systematic analysis of the complete MAVS 3'UTRs, or separate fragments, by using luciferase reporter assays or GFP fluorescence quantification, we observed significantly reduced luciferase reporter activity or fluorescent quenching in HEK293, HeLa and Hep G2 cells, as described for other 3'UTRs in previous studies [46]. By deletion analysis we identified the negative element located in region 1153-2145 that conferred a high instability effect in these cell lines (Fig. 1C). We also showed that negative elements in region 1153-2145 acted on the mRNA level and were dependent on the AREs (Fig. 2B). Moreover, our *in vitro* transcription and RNA pull-down assays showed that HuR, as one of the ARE-binding proteins, could bind to MAVS 3'UTR for regulating the mRNA (Fig. 2C and D). The HuR belongs to the group of proteins termed turnover and translation regulatory RNA-binding proteins [47] that mostly ensure the stabilization of a wide variety of mRNAs [29,31,48]. We speculated that HuR destabilizes MAVS mRNA by combining to a specific secondary structure (stem-loop) in the MAVS 3'UTR H1 fragment (region 1-3445 in the 3'UTR) to maintain the lower level of MAVS expression in resting cells, which was confirmed by the predicted result of the energy minimization program at the Mfold Web server [49] (Fig. S6). This interaction probably maintains the homeostasis of MAVS mRNA level in the host cells. Indeed, unstable mRNAs, including those encoding inflammatory mediators, cytokines, oncoproteins and G-coupled receptors, contain AREs in their 3'UTRs that promote the rapid degradation of mRNAs [50].

mRNA localization is a conserved post-transcriptional process of mitochondrial proteins and is crucial for a variety of systems [51,52]. The mitochondrial protein import process may begin ahead of recognizing the mitochondrial targeting signal [51], or a co-translational process is involved in the mitochondrial import [53]. We used the MAVS mRNA 3'UTR-induced GFP to show its role in cellular localization of MAVS mRNA to the vicinity of mitochondria, and found that the effect appeared to require *cis*-acting signals in region 5955-7687 (Fig. 3A–B). Similar to a previous observation that the yeast *ATM1* mRNA contains *cis*-acting signals in its 5' N-terminal region and 3'UTR, which direct heterologous RNA molecules to the vicinity of mitochondria *in vivo* [54]. mRNA targeting does not require translation of the 5'-sequence, suggesting that targeting occurs independent of translation and supporting the notion that the localization information can be encoded in the mRNA UTR rather than in the protein coding region [55]. As we did not perform the mRNA localization experiment by using the hybridization technique [53], further study will be carried out to confirm the pattern described here and to find out the exact regulatory elements in 3'UTR of MAVS for mitochondrial localization.

miRNA profiling studies have identified miRNAs whose expression was induced in cells upon RNA virus infections and this modulated the antiviral response by targeting the immune signaling pathways [56,57]. The role of miRNAs in the innate immune response had been demonstrated in the RLR signal pathway: miR-146a, as a negative feedback inhibitor, suppressed the RIG-I-dependent Type I IFN production in macrophages by targeting *TRAF6*, *IRAK1*, and *IRAK2* [58]. Nevertheless, to our knowledge, there are no reports of miRNA targeting MAVS 3'UTR. We found that miR-27a directly inhibited MAVS mRNA and protein expression (Figs. 4 and 5), which was firstly reported to be rapidly down-regulated in multiple mouse cell lines and in primary macrophages upon infection with the murine cytomegalovirus [59]. The miR-27a was up-regulated in response to virus infection and negatively regulated the MAVS-dependent IFN production (Fig. 6). During the preparation of this manuscript, Zheng et al. [60] reported that miR-27a was down-regulated in VSV infection by directly targeting Siglec1 and TRIM27, both of which were previously verified as negative

regulators of type I IFN, thus promoting VSV replication in macrophages. Nevertheless, there are critical differences in the mechanisms between these two studies: Firstly, Zheng et al. [60] showed that miR-27a expression was downregulated in primary peritoneal macrophages during different virus infections. However, miR-27a was up-regulated in HeLa cells in our study (Fig. 6A). Different cell type might have shown activation of different antiviral signal pathways with the same virus infection [61]. Secondly, we identified that MAVS 3'UTR was a direct target of miR-27a, when miR-27a was up-regulated upon virus infection, MAVS and its mediated signaling for the IFN production was negatively regulated, which finally promoted VSV replication (Fig. 6). However, Zheng et al. [60] showed that type I IFN-induced down-regulation of miR-27a could up-regulate Siglec1 and TRIM27 expression, with a feedback inhibition of the type I IFN production in antiviral innate response [60]. Taken together, the discrepancy of miR-27a effect on VSV invasion between Zheng et al. [60] and our study might be caused by different cell types used for assays and different targeting mRNAs highlighted by the virus infection. It should be mentioned that miR-326 was identified to have an upregulation effect on MAVS expression. Further study should be performed to answer whether miR-27a and miR-326 have a counteracting effect on balancing MAVS expression and how they affect the entire regulation network via MAVS in the cells.

In summary, we have shown that MAVS expression is precisely regulated at the post-transcriptional level via its long 3'UTR. This region contains regulatory elements and miRNA binding sites for modulating MAVS mRNA stability, protein expression and subcellular localization of protein to the vicinity of mitochondria. Our study provides a paradigm for understanding the complex role of 3'UTR in a key gene active in innate immunity.

## Transparency document

The Transparency document associated this article can be found, in online version.

## Acknowledgments

We thank Ian Logan for language editing and Miss Min Xu for help with the mRNA decay assay. This study was supported by the National Natural Science Foundation of China (U1402224 and 31001006), Yunnan Province (2016FB028) and the Western Light program of Chinese Academy of Sciences (中国科学院西部之光计划).

## Appendix A. Supplementary data

Supplementary data to this article can be found online at <https://doi.org/10.1016/j.bbagr.2018.10.017>.

## References

- [1] S. Akira, S. Uematsu, O. Takeuchi, Pathogen recognition and innate immunity, *Cell* 124 (2006) 783–801.
- [2] K. Honda, H. Yanai, A. Takaoka, T. Taniguchi, Regulation of the type I IFN induction: a current view, *Int. Immunol.* 17 (2005) 1367–1378.
- [3] E.L. Mills, B. Kelly, L.A.J. O'Neill, Mitochondria are the powerhouses of immunity, *Nat. Immunol.* 18 (2017) 488–498.
- [4] R.B. Seth, L. Sun, C.K. Ea, Z.J. Chen, Identification and characterization of MAVS, a mitochondrial antiviral signaling protein that activates NF-kappaB and IRF 3, *Cell* 122 (2005) 669–682.
- [5] T. Kawai, K. Takahashi, S. Sato, C. Coban, H. Kumar, H. Kato, K.J. Ishii, O. Takeuchi, S. Akira, IPS-1, an adaptor triggering RIG-I- and Mda5-mediated type I interferon induction, *Nat. Immunol.* 6 (2005) 981–988.
- [6] E. Meylan, J. Curran, K. Hofmann, D. Moradpour, M. Binder, R. Bartschlagler, J. Tschoopp, Cardif is an adaptor protein in the RIG-I antiviral pathway and is targeted by hepatitis C virus, *Nature* 437 (2005) 1167–1172.
- [7] L.G. Xu, Y.Y. Wang, K.J. Han, L.Y. Li, Z. Zhai, H.B. Shu, VISA is an adapter protein required for virus-triggered IFN-beta signaling, *Mol. Cell* 19 (2005) 727–740.
- [8] B. Qi, Y. Huang, D. Rowe, G. Halliday, VISA—a pass to innate immunity, *Int. J. Biochem. Cell Biol.* 39 (2007) 287–291.

- [9] N. Qi, Y. Shi, R. Zhang, W. Zhu, B. Yuan, X. Li, C. Wang, X. Zhang, F. Hou, Multiple truncated isoforms of MAVS prevent its spontaneous aggregation in antiviral innate immune signalling, *Nat. Commun.* 8 (2017) 15676.
- [10] Sky W. Brubaker, Anna E. Gauthier, Eric W. Mills, Nicholas T. Ingolia, Jonathan C. Kagan, A bicistronic MAVS transcript highlights a class of truncated variants in antiviral immunity, *Cell* 156 (2014) 800–811.
- [11] B. Liu, C. Gao, Regulation of MAVS activation through post-translational modifications, *Curr. Opin. Immunol.* 50 (2018) 75–81.
- [12] D. Day, M. Tuite, Post-transcriptional gene regulatory mechanisms in eukaryotes: an overview, *J. Endocrinol.* 157 (1998) 361–371.
- [13] J. Kong, P. Lasko, Translational control in cellular and developmental processes, *Nat. Rev. Genet.* 13 (2012) 383–394.
- [14] J.-R. Yang, Does mRNA structure contain genetic information for regulating co-translational protein folding? *Zool. Res.* 38 (2017) 36–43.
- [15] A. Bashirullah, R.L. Cooperstock, H.D. Lipshitz, Spatial and temporal control of RNA stability, *Proc. Natl. Acad. Sci. U. S. A.* 98 (2001) 7025–7028.
- [16] A.W. van der Velden, A.A. Thomas, The role of the 5' untranslated region of an mRNA in translation regulation during development, *Int. J. Biochem. Cell Biol.* 31 (1999) 87–106.
- [17] R.P. Jansen, mRNA localization: message on the move, *Nat. Rev. Mol. Cell Biol.* 2 (2001) 247–256.
- [18] F. Mignone, C. Gissi, S. Liuni, G. Pesole, Untranslated regions of mRNAs, *Genome Biol.* 3 (2002) (REVIEW0004).
- [19] D. Bartel, MicroRNAs genomics, biogenesis, mechanism, and function, *Cell* 116 (2004) 281–297.
- [20] L. He, G.J. Hannon, MicroRNAs: small RNAs with a big role in gene regulation, *Nat. Rev. Genet.* 5 (2004) 522–531.
- [21] A.S. Flynt, E.C. Lai, Biological principles of microRNA-mediated regulation: shared themes amid diversity, *Nat. Rev. Genet.* 9 (2008) 831–842.
- [22] L. Xu, D. Yu, Y. Fan, L. Peng, Y. Wu, Y.-G. Yao, Loss of RIG-I leads to a functional replacement with MDA5 in the Chinese tree shrew, *Natl. Acad. Sci. U. S. A.* 113 (2016) 10950–10955.
- [23] L. Xu, D. Yu, L. Peng, Y. Fan, J. Chen, Y.-T. Zheng, C. Wang, Y.-G. Yao, Characterization of a MAVS ortholog from the Chinese tree shrew (*Tupaia belangeri chinensis*), *Dev. Comp. Immunol.* 52 (2015) 58–68.
- [24] D. Yu, Y. Wu, L. Xu, Y. Fan, L. Peng, M. Xu, Y.-G. Yao, Identification and characterization of toll-like receptors (TLRs) in the Chinese tree shrew (*Tupaia belangeri chinensis*), *Dev. Comp. Immunol.* 60 (2016) 127–138.
- [25] A. Anantharaman, O. Gholamalamdari, A. Khan, J.H. Yoon, M.F. Jantsch, J.C. Hartner, M. Gorospe, S.G. Prasanth, K.V. Prasanth, RNA-editing enzymes ADAR1 and ADAR2 coordinately regulate the editing and expression of Ctn RNA, *FEBS Lett.* 591 (2017) 2890–2904.
- [26] G. Grillo, A. Turi, F. Licciulli, F. Mignone, S. Liuni, S. Banfi, V.A. Gennarino, D.S. Horner, G. Pavesi, E. Picardi, G. Pesole, UTRdb and UTRsite (RELEASE 2010): a collection of sequences and regulatory motifs of the untranslated regions of eukaryotic mRNAs, *Nucleic Acids Res.* 38 (2010) D75–D80.
- [27] B. Rattenbacher, P.R. Bohjanen, Evaluating posttranscriptional regulation of cytokine genes, in: M. De Ley (Ed.), *Cytokine Protocols*, Humana Press, Totowa, NJ, 2012, pp. 71–89.
- [28] A.M. Zubiaga, J.G. Belasco, M.E. Greenberg, The nonamer UUAUUUUUU is the key AU-rich sequence motif that mediates mRNA degradation, *Mol. Cell Biol.* 15 (1995) 2219–2230.
- [29] E. Matoukova, E. Michalova, B. Vojtesek, R. Hrstka, The role of the 3' untranslated region in post-transcriptional regulation of protein expression in mammalian cells, *RNA Biol.* 9 (2012) 563–576.
- [30] J. Fallmann, V. Sedlyarov, A. Tanzer, P. Kovarik, Ivo L. Hofacker, AREsite2: an enhanced database for the comprehensive investigation of AU/GU/U-rich elements, *Nucleic Acids Res.* 44 (2016) D90–D95.
- [31] S.M. García-Mauriño, F. Rivero-Rodríguez, A. Velázquez-Cruz, M. Hernández-Vellisca, A. Díaz-Quintana, M.A. De la Rosa, I. Díaz-Moreno, RNA binding protein regulation and cross-talk in the control of AU-rich mRNA fate, *Front. Mol. Biosci.* 4 (2017) 71.
- [32] I. Grammatikakis, K. Abdelmohsen, M. Gorospe, Posttranslational control of HuR function, *WIREs RNA* 8 (2017) (e1372-n/a).
- [33] T. Nishihara, L. Zekri, J.E. Braun, E. Izaurralde, miRISC recruits decapping factors to miRNA targets to enhance their degradation, *Nucleic Acids Res.* 41 (2013) 8692–8705.
- [34] N. Chang, J. Yi, G. Guo, X. Liu, Y. Shang, T. Tong, Q. Cui, M. Zhan, M. Gorospe, W. Wang, HuR uses AUF1 as a cofactor to promote p16<sup>INK4</sup> mRNA decay, *Mol. Cell Biol.* 30 (2010) 3875–3886.
- [35] M. Corral-Debrinski, mRNA specific subcellular localization represents a crucial step for fine-tuning of gene expression in mammalian cells, *Biochim. Biophys. Acta* 1773 (2007) 473–475.
- [36] J. Krol, I. Loedige, W. Filipowicz, The widespread regulation of microRNA biogenesis, function and decay, *Nat. Rev. Genet.* 11 (2010) 597–610.
- [37] V. Ambros, The functions of animal microRNAs, *Nature* 431 (2004) 350–355.
- [38] D.W. Trobaugh, W.B. Klimstra, MicroRNA regulation of RNA virus replication and pathogenesis, *Trend. Mol. Med.* 23 (2016) 80–93.
- [39] A. Krek, D. Grün, M.N. Poy, R. Wolf, L. Rosenber, E.J. Epstein, P. MacMenamin, I. da Piedade, K.C. Gunsalus, M. Stoffel, N. Rajewsky, Combinatorial microRNA target predictions, *Nat. Genet.* 37 (2005) 495.
- [40] V. Agarwal, G.W. Bell, J.-W. Nam, D.P. Bartel, Predicting effective microRNA target sites in mammalian mRNAs, *elife* 4 (2015) e05005.
- [41] B. John, A.J. Enright, A. Aravin, T. Tuschl, C. Sander, D.S. Marks, Human microRNA targets, *PLoS Biol.* 2 (2004) e363.
- [42] D. Goubau, S. Deddouche, C. Reis e Sousa, Cytosolic sensing of viruses, *Immunity* 38 (2013) 855–869.
- [43] P.J. Mitchell, R. Tjian, Transcriptional regulation in mammalian cells by sequence-specific DNA binding proteins, *Science* 245 (1989) 371–378.
- [44] J.T. Kadonaga, Regulation of RNA polymerase II transcription by sequence-specific DNA binding factors, *Cell* 116 (2004) 247–257.
- [45] M.J. Moore, From birth to death: the complex lives of eukaryotic mRNAs, *Science* 309 (2005) 1514–1518.
- [46] A. Wirsing, S. Senkel, L. Klein-Hitpass, G.U. Ryffel, A systematic analysis of the 3'UTR of HNF4A mRNA reveals an interplay of regulatory elements including miRNA target sites, *PLoS One* 6 (2011) e27438.
- [47] R. Pullmann Jr., H.H. Kim, K. Abdelmohsen, A. Lal, J.L. Martindale, X. Yang, M. Gorospe, Analysis of turnover and translation regulatory RNA-binding protein expression through binding to cognate mRNAs, *Mol. Cell Biol.* 27 (2007) 6265–6278.
- [48] B.L. Phillips, A. Banerjee, B.J. Sanchez, S. Di Marco, I.E. Gallouzi, G.K. Pavlath, A.H. Corbett, Post-transcriptional regulation of Pabpn1 by the RNA binding protein HuR, *Nucleic Acids Res.* 46 (2018) 7643–7661.
- [49] M. Zuker, Mfold web server for nucleic acid folding and hybridization prediction, *Nucleic Acids Res.* 31 (2003) 3406–3415.
- [50] C.T. Demaria, G. Brewer, AUF1 binding affinity to A+U-rich elements correlates with rapid mRNA degradation, *J. Biol. Chem.* 271 (1996) 12179–12184.
- [51] P. Marc, A. Margeot, F. Devaux, C. Blugeon, M. Corral-Debrinski, C. Jacq, Genome-wide analysis of mRNAs targeted to yeast mitochondria, *EMBO Rep.* 3 (2002) 159–164.
- [52] J. Sylvestre, A. Margeot, C. Jacq, G. Dujardin, M. Corral-Debrinski, The role of the 3' untranslated region in mRNA sorting to the vicinity of mitochondria is conserved from yeast to human cells, *Mol. Biol. Cell* 14 (2003) 3848–3856.
- [53] A. Loya, L. Pnueli, Y. Yosefzon, Y. Wexler, M. Ziv-Ukelson, Y. Arava, The 3'-UTR mediates the cellular localization of an mRNA encoding a short plasma membrane protein, *RNA* 14 (2008) 1352–1365.
- [54] M. Corral-Debrinski, C. Blugeon, C. Jacq, In yeast, the 3' untranslated region or the presequence of ATM1 is required for the exclusive localization of its mRNA to the vicinity of mitochondria, *Mol. Cell Biol.* 20 (2000) 7881–7892.
- [55] H. Jung, Christos G. Gkogkas, N. Sonenberg, Christine E. Holt, Remote control of gene function by local translation, *Cell* 157 (2014) 26–40.
- [56] M.L. Yarbrough, K. Zhang, R. Sakthivel, C.V. Forst, B.A. Posner, G.N. Barber, M.A. White, B.M. Fontoura, Primate-specific miR-576-3p sets host defense signaling threshold, *Nat. Commun.* 5 (2014) 4963.
- [57] W.A. Buggele, K.E. Johnson, C.M. Horvath, Influenza A virus infection of human respiratory cells induces primary microRNA expression, *J. Biol. Chem.* 287 (2012) 31027–31040.
- [58] J. Hou, P. Wang, L. Lin, X. Liu, F. Ma, H. An, Z. Wang, X. Cao, MicroRNA-146a feedback inhibits RIG-I-dependent type I IFN production in macrophages by targeting TRAF6, IRAK1, and IRAK2, *J. Immunol.* 183 (2009) 2150–2158.
- [59] A.H. Buck, J. Perot, M.A. Chisholm, D.S. Kumar, L. Tuddenham, V. Cognat, L. Marcinowski, L. Dölken, S. Pfeffer, Post-transcriptional regulation of miR-27 in murine cytomegalovirus infection, *RNA* 16 (2010) 307–315.
- [60] Q. Zheng, J. Hou, Y. Zhou, Y. Yang, X. Cao, Type I IFN-inducible downregulation of microRNA-27a feedback inhibits antiviral innate response by upregulating Siglec1/TRIM27, *J. Immunol.* 196 (2016) 1317–1326.
- [61] Y. Ran, H.B. Shu, Y.Y. Wang, MITA/STING: a central and multifaceted mediator in innate immune response, *Cytokine Growth Factor Rev.* 25 (2014) 631–639.

Supplementary files

**Table S1. Primers for constructing vectors and performing real-time quantitative PCR (RT-qPCR)**

Primer	Sequence (5'-3')	Restriction endonuclease	Application and vector
hBspE-1F	CGG <u>TCCGGAT</u> GAAAGCCCTGGGCTCTTC	<i>BspE</i> I	PCR for constructing pCS-EGFP-H1 using
hXba-1R	GCG <u>TCTAGAG</u> GTTTGGGTGCAGTGTC	<i>Xba</i> I	pCS-EGFP vector
hBspE-2F	CGG <u>TCCGGAG</u> GTTGGCCTCATGAGATC	<i>BspE</i> I	PCR for constructing pCS-EGFP-H2 using
hXba-2R	GC <u>TCTAGACT</u> GCCCCACTTCATATT	<i>Xba</i> I	pCS-EGFP vector
hXba-3F	CGG <u>TCCGGAC</u> AGGCTAAGGTGTTTCAT	<i>BspE</i> I	PCR for constructing pCS-EGFP-H3 using
hXba-3R	GC <u>TCTAGAT</u> AGAAGTAATAATAGCAG	<i>Xba</i> I	pCS-EGFP vector
hXba-4F	CGG <u>TCCGGAG</u> TATGTAGCCCCGAAGAC	<i>BspE</i> I	PCR for constructing pCS-EGFP-H4 using
hXba-4R	GC <u>TCTAGACT</u> TCACTCTCCAACTTC	<i>Xba</i> I	pCS-EGFP vector
hXba-5F	CGG <u>TCCGGAT</u> GAAACCACAGCTTATCAC	<i>BspE</i> I	PCR for constructing pCS-EGFP-H5 using
hXba-5R	GC <u>TCTAGAG</u> TTTTCCAACAGGGTCAC	<i>Xba</i> I	pCS-EGFP vector
hBspE-1197F	CGG <u>TCCGGAT</u> TGGCATTACCAAGGGTTG	<i>BspE</i> I	PCR for constructing pCS-EGFP-H1-3
hXba-1R	GCG <u>TCTAGAG</u> GTTTGGGTGCAGTGTC	<i>Xba</i> I	(1197-3445) using pCS-EGFP vector
hBspE-1F	CGG <u>TCCGGAT</u> GAAAGCCCTGGGCTCTTC	<i>BspE</i> I	PCR for constructing pCS-EGFP-H1-1 (1-1160)
hXba-1160R	CGG <u>TCTAGAC</u> ATCGATAAACTCCTTTA	<i>Xba</i> I	using pCS-EGFP vector
hBspE-2308F	CGG <u>TCCGGAT</u> GAAACCCCGTCTCTAC	<i>BspE</i> I	PCR for constructing pCS-EGFP-H1-4
hXba-1R	GCG <u>TCTAGAG</u> GTTTGGGTGCAGTGTC	<i>Xba</i> I	(2308-3445) using pCS-EGFP vector
hBspE-1F	CGG <u>TCCGGAT</u> GAAAGCCCTGGGCTCTTC	<i>BspE</i> I	PCR for constructing pCS-EGFP-H1-2 (1-2145)
hXba-2145R	G <u>TCTAGAC</u> GGTAATACAATAAAACT	<i>Xba</i> I	using pCS-EGFP vector
hBspE-1153F	CGG <u>TCCGGAT</u> GAAAGATTAAAGGAGTT	<i>BspE</i> I	PCR for constructing pCS-EGFP-H1-5
hXba-2145R	G <u>TCTAGAC</u> GGTAATACAATAAAACT	<i>Xba</i> I	(1153-2145) using pCS-EGFP vector

UD1152-2145	TTTGTAGAGACGGGGTTTCCAACACTGGGAAATATA		PCR for constructing pCS-EGFP-H1-6
LD1152-2145	TATATATATTTCCCAGTGTTGGAAACCCCGTCTCTAC		( $\Delta$ 1153-2145) using pCS-EGFP vector
UD957-2145	GCCCAACAGTTTTATTGTATTACCGTTC		PCR for constructing $\Delta$ 957-2145 using
LD957-2145	GAACGGTAATACAATAAAACTGTTGGGC		pCS-EGFP-H1 vector
H1-1069F	TTGGGCAAGGGATCTATCTGTCTGTC		PCR for constructing 3ARE-mutant of site 1
H1-1069R	GACAGACAGATAGATCCCTTGCCCAA		(1080-1084) using pCS-EGFP-H1 vector
H1-1191F	GAGTCCTGGCATCTACCAAGGGTTGG		PCR for constructing 3ARE-mutant of site 2
H1-1191R	CCAACCCTTGGTAGATGCCAGGACTC		(1201-1205) using pCS-EGFP-H1 vector
H1-2128F	AGTTAACAATCTATGCACAGGTA		PCR for constructing 3ARE-mutant of site 3
H1-2128R	TAGTACCTGTGCATAGATTGTTAACT		(2128-2132) using pCS-EGFP-H1 vector
hXhoI-1F	CCGCTCGAGTGAAGCCCTGGGCTCTTC	<i>Xho</i> I	PCR for constructing psiCHECK-2-H1 using
hNotI-1R	ATAAGAATGCGGCCGCGTGGGTGCAGTGTC	<i>Not</i> I	psiCHECK-2 vector
hXhoI -2F	CCGCTCGAGATACTATAATCCCAGCA	<i>Xho</i> I	PCR for constructing psiCHECK-2-h2 using
hNotI -2R	ATAAGAATGCGGCCGCTAGAAGTAATAATAGCAG	<i>Not</i> I	psiCHECK-2 vector
hXhoI -3F	CCGCTCGAGTCATGAGATCTTGCCTTA	<i>Xho</i> I	PCR for constructing psiCHECK-2-h3 using
hNotI -3R	ATAAGAATGCGGCCGCCAACATATGAATTCAAAG	<i>Not</i> I	psiCHECK-2 vector
hXhoI-1F	CCGCTCGAGTGAAGCCCTGGGCTCTTC	<i>Xho</i> I	PCR for constructing psiCHECK-2-h using
hNotI -3R	ATAAGAATGCGGCCGCCAACATATGAATTCAAAG	<i>Not</i> I	psiCHECK-2 vector
hXhoI-1F	CCGCTCGAGTGAAGCCCTGGGCTCTTC	<i>Xho</i> I	PCR for constructing pBluescript-H1 using
hNotI-1R	ATAAGAATGCGGCCGCGTGGGTGCAGTGTC	<i>Not</i> I	pBluescript vector
hXhoI -2F	CCGCTCGAGATACTATAATCCCAGCA	<i>Xho</i> I	PCR for constructing pBluescript-h2 using
hNotI -2R	ATAAGAATGCGGCCGCTAGAAGTAATAATAGCAG	<i>Not</i> I	pBluescript vector
hXhoI -3F	CCGCTCGAGTCATGAGATCTTGCCTTA	<i>Xho</i> I	PCR for constructing pBluescript-h3 using
hNotI -3R	ATAAGAATGCGGCCGCCAACATATGAATTCAAAG	<i>Not</i> I	pBluescript vector
hXhoI-1F	CCGCTCGAGTGAAGCCCTGGGCTCTTC	<i>Xho</i> I	PCR for constructing pBluescript-h using

hNotI -3R	ATAAGAAT <u>GCGGCCGCC</u> CAACATATGAATTCAAAG	<i>Not I</i>	pBluescript vector
UD957-2145	GCCCAACAGTTTTATTGTATTACCGTTC		PCR for constructing $\Delta$ 957-2145 ( $\Delta$ 957-2145)
LD957-2145	GAACGGTAATACAATAAAACTGTTGGGC		using pBluescript-H1 vector
H1-1069F	TTGGGCAAGGGATCTATCTGTCTGTC		PCR for constructing 3ARE-mutant of site 1
H1-1069R	GACAGACAGATAGATCCCTTGCCCAA		(1080-1084) using pBluescript-H1 vector
H1-1191F	GAGTCCTGGCATCTACCAAGGGTTGG		PCR for constructing 3ARE-mutant of site 2
H1-1191R	CCAACCCTTGGTAGATGCCAGGACTC		(1201-1205) using pBluescript-H1 vector
H1-2128F	AGTTAACAATCTATGCACAGGTA		PCR for constructing 3ARE-mutant of site 3
H1-2128R	TAGTACCTGTGCATAGATTGTAACT		(2128-2132) using pBluescript-H1 vector
psiCHECK-h-660L	GGCCTATGAGACTGCTCTGCACATGTAGGT		PCR for constructing M1 using psiCHECK-2
psiCHECK-h-660U	ACCTACATGTGCAGAGCAGTCTCATAGGCC		vector
psiCHECK-h-1563L	TTATTTCTGAGACTTCTAGAGGCTGGGAAG		PCR for constructing M2 using psiCHECK-2
psiCHECK-h-1563U	CTTCCCAGCCTCTAGAAGTCTCAGAAATAA		vector
psiCHECK-h-2295L	CTATAACATTTGAGACTCCCTGCCTGCCTT		PCR for constructing M3 using psiCHECK-2
psiCHECK-h-2295U	AAGGCAGGCAGGGAGTCTCAAATGTTATAG		vector
psiCHECK-h-3499L	GTCCAGCCTGAGACTTTACAGGTCCTGGAG		PCR for constructing M4 using psiCHECK-2
psiCHECK-h-3499U	CTCCAGGACCTGTAAAGTCTCAGGCTGGAC		vector
pCMV mir-27a-F:	GAG <u>GCGATCG</u> CGCATATGAGAAAAGAGCT	<i>Sgf I</i>	PCR for constructing pCMV-miR-27a using
pCMV mir-27a-R	GCG <u>ACGCGT</u> CCUGCAGCACACAUUUGG	<i>Mlu I</i>	pCMV-MIR precursors
MAVS-F	TAAGTCCGAGGGCACCTTTGG		Analytical RT-qPCR for <i>MAVS</i> mRNA level
MAVS-R	CCTCCCTCTCCTGGA		
EGFP-F	TACAACTACAACAGCCACAA		Analytical RT-qPCR for <i>GFP</i> mRNA level
EGFP-R	CGGATCTTGAAGTTCACCTT		
IFNB1-F	TCAGAGTGGAAATCCTAAGG		Analytical RT-qPCR for <i>IFNB1</i> mRNA level
IFNB1-R	CTGGTTGAAGAATGCTTGAA		

---

GAPDH-F	CAACTACATGGTTTACATGTTC
GAPDH-R	GCCAGTGGACTCCACGAC

---

Analytical RT-qPCR for *GAPDH* mRNA level [1]

## Reference

[1] S. Zhou, S. Kachhap, W. Sun, G. Wu, A. Chuang, L. Poeta, L. Grumbine, S.K. Mithani, A. Chatterjee, W. Koch, W.H. Westra, A. Maitra, C. Glazer, M. Carducci, D. Sidransky, T. McFate, A. Verma, J.A. Califano, Frequency and phenotypic implications of mitochondrial DNA mutations in human squamous cell cancers of the head and neck, *Proc. Natl. Acad. Sci. U. S. A.* **104**, 2007, 7540-7545.

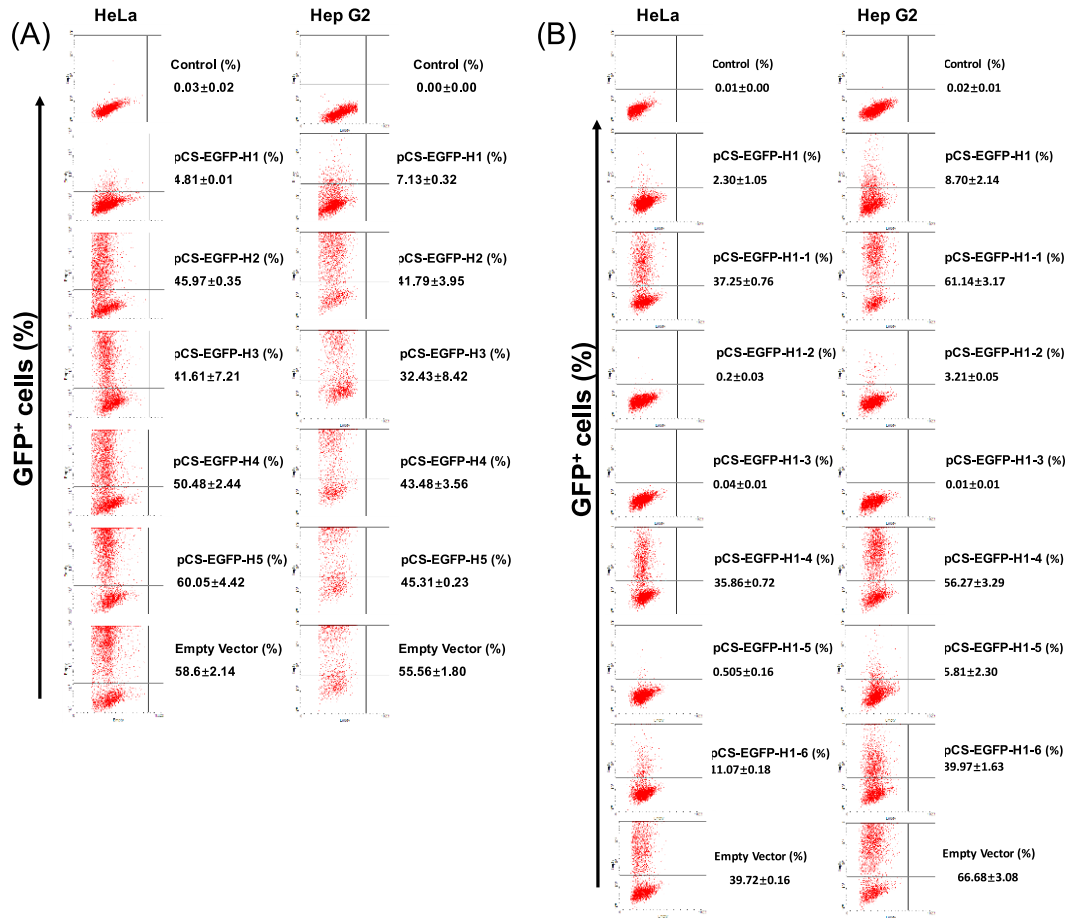


**Figure S1. Characterization of the potential regulatory elements in human *MAVS* 3'UTR.** (A) Flow cytometry analyses of cells with transfection of vectors containing *MAVS* 3'UTR truncated fragments (pCS-EGFP-H1 1-3445, pCS-EGFP-H2 3372-6832, pCS-EGFP-H3 6789-9976, pCS-EGFP-H4 2505-5051 and pCS-EGFP-H5 5955-7687). The HeLa or Hep G2 cells ( $1 \times 10^5$ ) were transfected with the indicated expression vector ( $1 \mu\text{g}$ ) for 48 h before harvest for flow cytometry analysis. (B) Characterization of the putative inhibitory elements in the *MAVS* 3'UTR fragment H1. The *MAVS* 3'UTR fragment H1 was truncated into 5 fragments or introduced with a deletion of 992 bp. The procedure was similar to (A). All experiments were repeated three times with similar results.



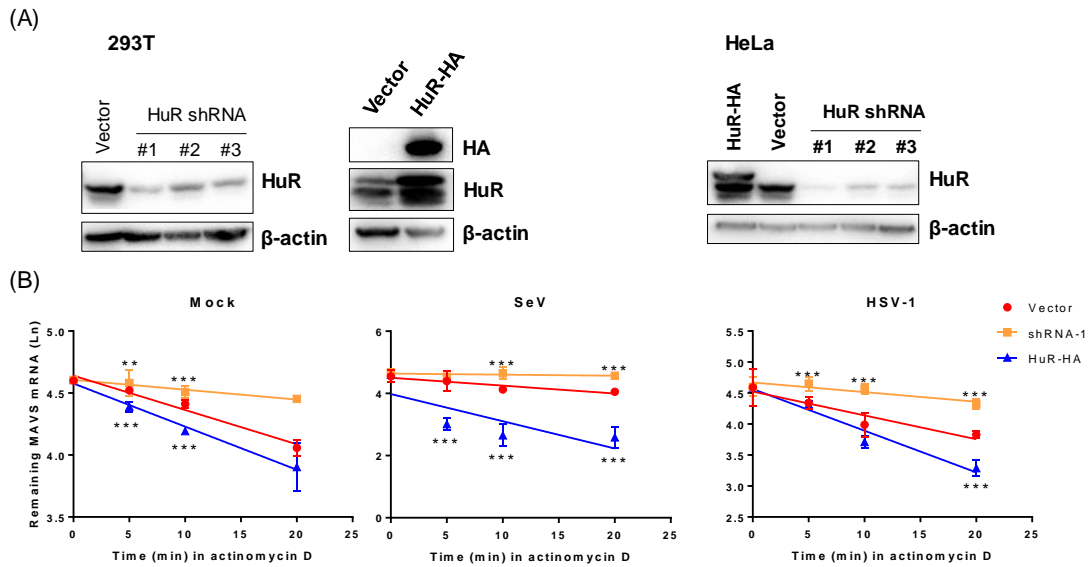


**Figure S3. HuR represses MAVS expression in resting cells or cells infected with SeV and HSV-1.** (A) Overexpression and knockdown of HuR in HEK293 and HeLa cells. Cells ( $1 \times 10^5$ ) were transfected with HuR-HA expression vector (1  $\mu$ g), HuR shRNA-1 (1  $\mu$ g), HuR shRNA-2 (1  $\mu$ g), HuR shRNA-3 (1  $\mu$ g) lentivirus vectors and empty vector (Vector, 1  $\mu$ g). Cells were harvested at 48 h after transfection and cell lysates were analyzed for HuR protein levels, which were quantified by Western blot using antibody for HuR. The  $\beta$ -actin was used as loading control. HuR shRNA-1 lentivirus vector had the highest inhibitory efficiency in both cell lines and was used to in the subsequent experiments. (B) Overexpression or knockdown of HuR affected *MAVS* mRNA half-life in HeLa cells with or without SeV and HSV-1 infection. Cells ( $1 \times 10^4$ ) were cultured in a 24-well plate and transfected with overexpression vector (HuR-HA) or HuR shRNA-1 (each 0.5  $\mu$ g) and the empty vector (Vector, 0.5  $\mu$ g) for 36 h, followed by infection without or with SeV (25 HAU/mL), HSV-1 (MOI=10) for 9 h, then cells were treated with or without Actinomycin D (5  $\mu$ g/mL) at the indicated times before the harvest. Total RNA was extracted from the transfected cells and the mRNA level of *MAVS* was measured by using the RT-qPCR, with normalization to the level of *GAPDH*. \*  $P < 0.05$ , \*\*  $P < 0.01$ , \*\*\*  $P < 0.001$ , Student's  $t$  test. Bars represent mean  $\pm$  SEM. All experiments were repeated three times with similar results.

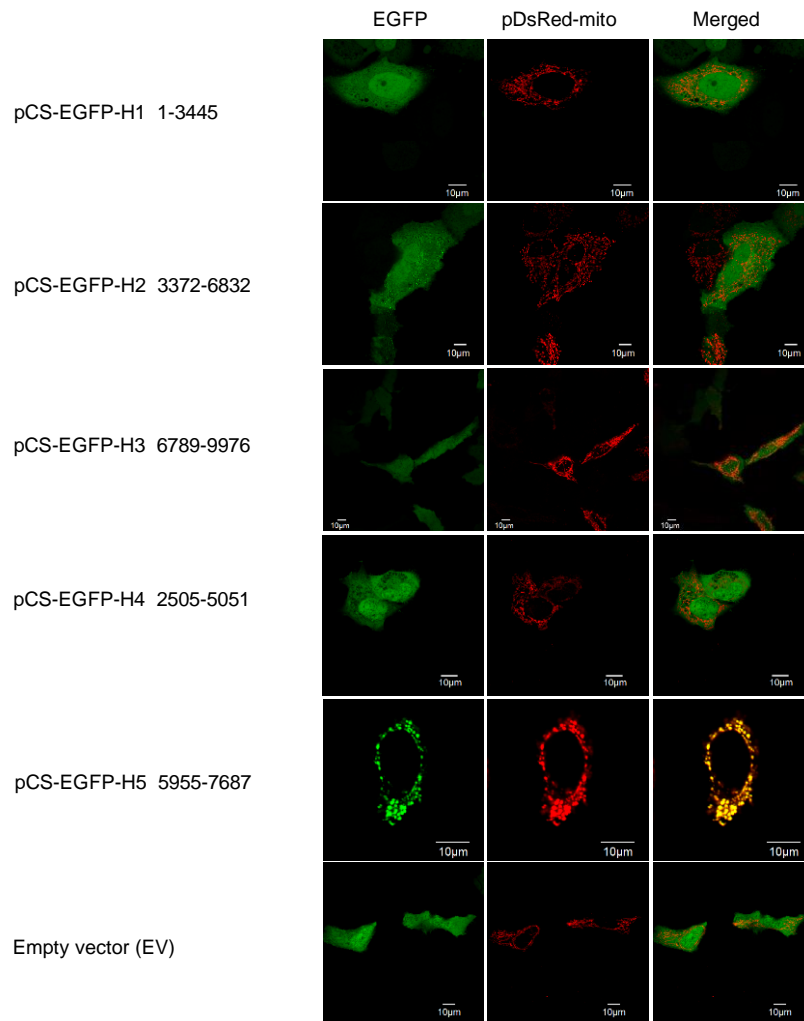


**Figure S4. Localization of EGFP in Hep G2 cells transfected with pCS-EGFP expression vectors with different fragments of MAVS 3'UTR.** Hep G2 cells ( $1 \times 10^5$ ) were cultured on glass slides in a 12-well plate and were co-transfected with pDsRed-mito vector (0.1  $\mu\text{g}$ ) and the indicated MAVS 3'UTR expression vector (1  $\mu\text{g}$ ) containing MAVS 3'UTR truncated fragment (pCS-EGFP-H1 1-3445, pCS-EGFP-H2 3372-6832, pCS-EGFP-H3 6789-9976, pCS-EGFP-H4 2505-5051 and pCS-EGFP-H5 5955-7687) for 48 h. Living cells were imaged using the Olympus FluoView 1000 confocal microscope at 488 nm and 563 nm, respectively.

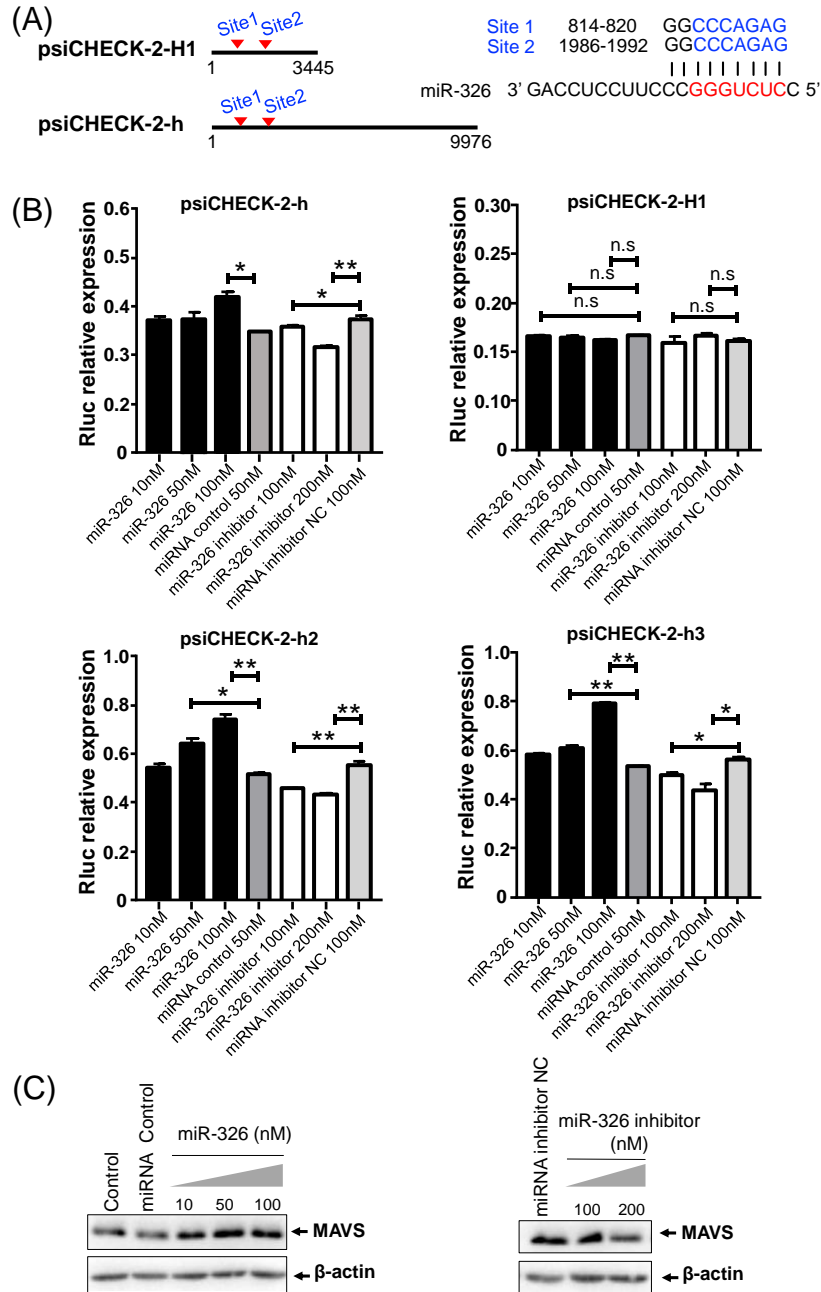


**Figure S5. miR-326 indirectly targeted to the MAVS 3'UTR.** (A) The miR-326 binding sites in fragments H1 of the MAVS 3'UTR. The red labels indicated the miR-326 binding sites in MAVS 3'UTR fragments H1 and h that were inserted into psiCHECK-2 vector. (B) The enhancing effect of miR-326 on the MAVS 3'UTR presents a dose-dependent manner. HEK293 cells ( $1 \times 10^4$ ) were transfected with the indicated reporter vector (psiCHECK-2-h, psiCHECK-2-H1, psiCHECK-2-h2 or psiCHECK-2-h3), together with different concentrations of miR-326 mimics or miR-326 inhibitors. Cells were lysed and detected for luciferase activity at 48 h after transfection. miRNA control and miRNA inhibitor control (miRNA inhibitor NC) were used as negative controls. (C) Effect of miR-326 on endogenous MAVS protein expression. HEK293 cells ( $1 \times 10^5$ ) were transfected with the miR-326 inhibitor (100 nM, 200 nM), miRNA inhibitor NC (100 nM), miRNA control (100 nM), or miR-326 mimics (10 nM, 50 nM and 100 nM). Cells were harvested at 48 h after transfection and the endogenous MAVS was detected by Western blot. Immunoblot for  $\beta$ -actin was used as loading control. n.s. - not significant, \*  $P < 0.05$ , \*\*  $P < 0.01$ , Student's *t* test. Bars represent mean  $\pm$  SEM. The experiments were repeated three times with similar results.

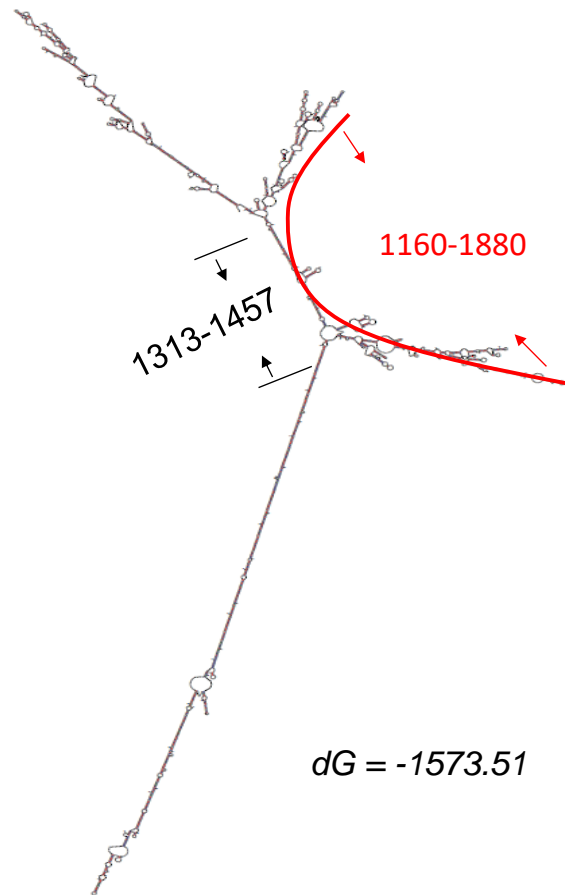


**Figure S6. The predicted secondary structure of the *MAVS* 3'UTR fragment H1.** The secondary structure was predicted by using the energy minimization program of the Mfold Web server (<http://unafold.rna.albany.edu/?q=mfold>). Red-loop and red arrows indicated the secondary structure of region 1160-1880 that was located in fragment H1. Black arrows indicated the secondary structure of region 1313-1457 in the bottom of red-loop (region 1160-1880).